REPORT DOCUMENTATION PAGE	Form Approved OMB NO. 0704-0188

1. AGENCY USE ONLY (Leave Blank)	2. REPORT DATE September 3, 2004	3. REPORT TYPE AND DATES COVERED Final Report 03/15/2001 06/30/2004

4. TITLE AND SUBTITLE
Effective Use of Weld Metal Hydrogen Trapping and Advance Diffusible Hydrogen Sensing

5. FUNDING NUMBERS
DAAD19-01-1-0377

6. AUTHOR(S)
David L. Olson and Yeong-Do Park

7. PERFORMING ORGANIZATION NAME(S) AND ADDRESS(ES)
Colorado School of Mines
Dept. Met. Mat. Engr.
Center for Welding, Joining, and Coating Research
Golden, Colorado 80401-1887

8. PERFORMING ORGANIZATION REPORT NUMBER
CSM-MT-CWJCR-004-026

9. SPONSORING / MONITORING AGENCY NAME(S) AND ADDRESS(ES)

U. S. Army Research Office
P.O. Box 12211
Research Triangle Park, NC 27709-2211

10. SPONSORING / MONITORING AGENCY REPORT NUMBER

41922.25-MS

11. SUPPLEMENTARY NOTES

12 a. DISTRIBUTION / AVAILABILITY STATEMENT

Approved for public release; distribution unlimited.

12 b. DISTRIBUTION CODE

13. ABSTRACT (Maximum 200 words)

The development of an advance measuring apparati for diffusible hydrogen content based on electronic, optical and magnetic property measurements was investigated. The effort was to develop a rapid and accurate detemination for both steel weld metal diffusible hydrogen content and its distribution. This investigation used the instrumentation acquired by the DURIP grant program. Thermoelectric (Seebeck) coefficient measurements are used to assess hydrogen content in higher strength low alloy steel, nickel-aluminum bronze, austenitic stainless steel, and hydrogen storage alloys. The thermoelectric power coefficient was also used to assess the soluble nitrogen content and nitride content in nitrogen strengthened structural steels.

The role of hydrogen to assist high temperature forming (defomation) was investigated in ferrous and refractory alloys. The investigation sought a mechanistic understanding for the significant reduction of compressive stress to hot form hydrogen charged ferrous alloys and refractory alloys.

Efforts were made to transfer the demonstrated effectiveness of weld metal hydrogen trapping, which results from investigation on rare earth additions to steel weld metal to lower the weld diffusible hydrogen content, to commercial welding practice and consumable products.

14. SUBJECT TERMS
Hydrogen Cracking, Diffusible Hydrogen, HSLA steel, Thermoelectric Power, Nitrogen Content

15. NUMBER OF PAGES
40

16. PRICE CODE

17. SECURITY CLASSIFICATION OR REPORT UNCLASSIFIED	18. SECURITY CLASSIFICATION ON THIS PAGE UNCLASSIFIED	19. SECURITY CLASSIFICATION OF ABSTRACT UNCLASSIFIED	20. LIMITATION OF ABSTRACT UL

NSN 7540-01-280-5500

Standard Form 298 (Rev.2-89)
Prescribed by ANSI Std. 239-18
298-102

20041102 091

BEST AVAILABLE COPY

GENERAL INSTRUCTIONS FOR COMPLETING SF 298

The Report Documentation Page (RDP) is used for announcing and cataloging reports. It is important that this information be consistent with the rest of the report, particularly the cover and title page. Instructions for filling in each block of the form follow. It is important to ***stay within the lines*** to meet ***optical scanning requirements.***

Block 1. Agency Use Only (Leave blank)

Block 2. Report Date. Full publication date including day, month, and year, if available (e.g. 1 Jan 88). Must cite at least year.

Block 3. Type of Report and Dates Covered. State whether report is interim, final, etc. If applicable enter inclusive report dates (e.g. 10 Jun 87 - 30 Jun 88).

Block 4. Title and Subtitle. A title is taken from the part of the report that provides the most meaningful and complete information. When a report is prepared in more than one volume, repeat the primary title, and volume number, and include subtitle for the specific volume. On classified documents enter the title classification in parentheses.

Block 5. Funding Numbers. To include contract and grant numbers; may include program element number(s) project number(s), task number(s), and work unit number(s). Use the following labels:

C - Contract
G - Grant
PE - Program Element
PR - Project
TA - Task
WU - Work Unit Accession No.

Block 6. Author(s). Name(s) of person(s) responsible for writing the report, performing the research, or credited with the content of the report. If editor or compiler, this should follow the name(s).

Block 7. Performing Organization Name(s) and Address(es). Self-explanatory.

Block 8. Performing Organization Report Number. Enter the unique alphanumeric report number(s) assigned by the organization performing the report.

Block 9. Sponsoring/Monitoring Agency Name(s) and Address(es) Self-explanatory.

Block 10. Sponsoring/Monitoring Agency Report Number. *(if known)*

Block 11. Supplementary Notes. Enter information not included elsewhere such as; prepared in cooperation with....; Trans. of...; To be published in.... When a report is revised, include a statement whether the new report supersedes or supplements the older report.

Block 12a. Distribution/Availability Statement. Denotes public availability or limitations. Cite any availability to the public. Enter additional limitations or special markings in all capitals (e.g. NORFORN, REL, ITAR).

DOD - See DoDD 4230.25, "Distribution Statements on Technical Documents."
DOE - See authorities.
NASA - See Handbook NHB 2200.2.
NTIS - Leave blank.

Block 12b. Distribution Code.

DOD - Leave Blank
DOE - Enter DOE distribution categories from the Standard Distribution for unclassified Scientific and Technical Reports
NASA - Leave Blank.
NTIS - Leave Blank.

Block 13. Abstract. Include a brief (*Maximum 200 words)* factual summary of the most significant information contained in the report.

Block 14. Subject Terms. Keywords or phrases identifying major subject in the report.

Block 15. Number of Pages. Enter the total number of pages.

Block 16. Price Code. Enter appropriate price code (NTIS *only*).

Block 17. - 19. Security Classifications. Self-explanatory. Enter U.S. Security Regulations (i.e., UNCLASSIFIED). If form contains classified information, stamp classification on the top and bottom of the page.

Block 20. Limitation of Abstract. This block must be completed to assign a limitation to the abstract. Enter either UL (Unlimited) or SAR (same as report). An entry in this block is necessary if the abstract is to be limited. If blank, the abstract is assumed to be unlimited.

Table of Contents

1. INTRODUCTION

1.1 Hydrogen Behavior in Metals and Alloys
1.2 Implication of Hydrogen Behavior
    1.2.1 Detrimental Effects of Hydrogen
    1.2.2 Hydrogen Management in Steel Weldments
    1.2.3 Beneficial Opportunities from Hydrogen

1.3 Nitrogen Behavior in Metal and Alloys
    1.3.1 Effect of Nitrogen Solubility on Weld Metal Nitrogen Content
    1.3.2 Beneficial Effect of Nitrogen
    1.3.3 Detrimental Effects of Nitrogen

2. SUMMARY OF THE IMPORTANT RESULTS DURING THIS CONTRACT

2.1 Thermoelectric Power Coefficient for Sensing of Hydrogen in Alloys.
    2.1.1 Thermodynamic Interpretation of TEP Correlation to Hydrogen Content
    2.1.2 Assessment to Hydrogen Content in Structural Alloys
    2.1.3 Assessment of Hydrogen Storage Capability

2.2 Hydrogen as a Transition Alloying Addition
    2.2.1 Invar Investigation
    2.2.2 Hydrogen Assisted Forming
    2.2.3 Hydrogen Induced Plastic Deformation in Ti-Nb Alloys

2.3 Hydrogen Management in Structural Alloy Welds
    2.3.1 Hydrogen Trapping as a Method to Manage Weld Metal Hydrogen Damage
    2.3.2 Irreversible Hydrogen Trapping in High Strength Steel Weldments

2.4 Thermoelectric Power Sensor to Assess Nitrogen Content

2.5 References

3. ACCOMPLISHMENTS OF THIS RESEARCH CONTRACT

4. COLLABORATIONS

5. LIST OF PUBLICATIONS FROM THIS RESEARCH CONTRACT

6. LIST OF ALL PARTICIPATING SCIENTIFIC PERSONNEL

1.0 INTRODUCTION

Understanding the role of hydrogen and nitrogen in defense related structural alloys is the essential foundation for the proper processing, design, use and integrity management of many specialty alloys. These specialty alloys include high strength steel used in numerous defense applications and nitrogen strengthened stainless steel used in some foreign submarine hulls because of its high strength and low magnetic signature. However, the addition of hydrogen and nitrogen can be both beneficial and detrimental to the mechanical properties and integrity of metals and alloys.

This final report describes beneficial attributes of experimental results during this contract period in structural materials. There are four activity areas and each activity area has tasks that are either completed and near completion. The four areas of activity include the following:

- Thermoelectric Power (TEP) Measurements for the Sensing of Hydrogen in Alloys (Section 2.1)
- Hydrogen as a Transient Alloying Addition (Section 2.2)
- Hydrogen Management in Structural Alloys and Their Welds (Section 2.3)
- Thermoelectric Power (TEP) Sensor to assess Soluble Nitrogen Content in Nitrogen Strengthened Stainless Steels (Section 2.4)

Section 3 is the list of accomplishments.

1.1 Hydrogen Behavior in Metals and Alloys

When hydrogen is introduced to an alloy it becomes an electron acceptor or an electron donor depending on primary solvent elements. Elements to the left of manganese on the periodic table give an electron to the hydrogen atom and it becomes negative causing the negative hydrogen ion to stay very localized to the metal donor atom resulting in hydride formation. For elements to the right of manganese, hydrogen will donate its electron to the metal *d*-band and it effectively becomes a proton in the nature of hydrogen in an alloy, which can be related to solution thermodynamic concepts. The heat of mixing of hydrogen in the metal also carries information as to whether an alloy is a major hydride former or whether the hydrogen is in solid solution. A heat of mixing of hydrogen in solid solution, which is negative, suggests hydrogen as an electron acceptor promoting localization behavior or even hydride formation. A heat of mixing that is positive suggests that hydrogen is in solution.

Hydrogen in the protonic state is known as soluble hydrogen, which usually has a high mobility. Hydrogen as a proton in the lattice has interactions with dislocations and thus change the mechanical behavior. It is this electron donor role for hydrogen that is the primary opportunity in this proposal because it offers the possibility for hydrogen to affect materials processing, influence alloy stability, and to allow electronic and magnetic property measurements to be used to rapidly assess alloy structure, properties, and stability.

Figure 1 illustrates the electron distribution for three cases [1]. The left diagram is the electronic distribution for a transition metal with no absorbed hydrogen. The center diagram is for a transition metal or alloy with electron donation from hydrogen absorption, with donated electrons primarily in the *d*-bands. The right diagram illustrates donations to the *d*-band, as well as some electrons becoming localized with the *sp*-band causing the formation of a metal hydride. The right diagram exhibits the desired behavior for a hydrogen storage electrode for a reversible battery. The middle diagram represents the situation of steel where the protonic hydrogen is behaving as soluble hydrogen. This solute hydrogen, if highly diffusible, is related with hydrogen assisted cracking in high strength low alloy steels (HSLA steels). It is this diffusible hydrogen that is associated with the service life of gun barrels.

The hydrogen interaction with most crystalline and amorphous transition metal alloys can be modeled with concepts illustrated in the center diagram. In a solid solution made up primarily of those elements to the right of the manganese of the transition metal series, the hydrogen atoms give their electrons to the d-band and thus become mobile protons in the lattice. This model agrees with most of the recent understanding of hydrogen transport in steels. This alteration of the d-band can change the magnetic susceptibility and, vice versa, the magnetic field can alter the filling of the *d*-states in such a way as to alter the solubility of diffusible hydrogen [2].

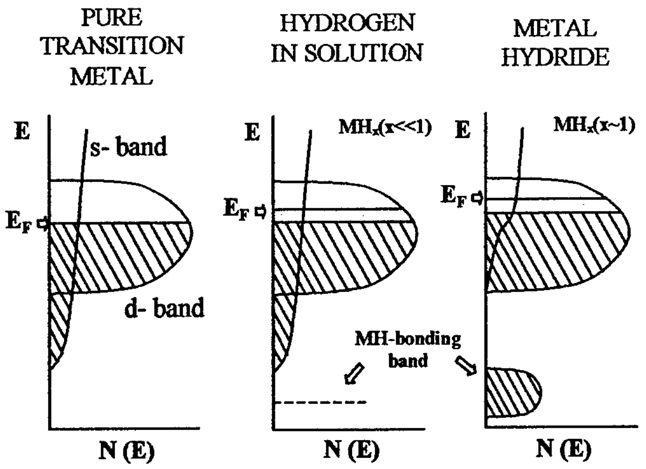

Figure 1 – Electronic structure of transition metal alloy with the introduction of hydrogen [1].

1.2 Implication of Hydrogen Behavior

Hydrogen exhibits both detrimental effects and beneficial opportunities as a solute in engineering alloys. Much effort has been given over the last fifty years to manage the detrimental effects. With better knowledge of the electronic and elastic interactions of hydrogen in materials, new opportunities are introduced for the enhancement of hydrogen behavior.

1.2.1 Detrimental Effects of Hydrogen

Hydrogen has been well known for its deleterious effects on steel weldments, such as the occurrence of cracking, particularly occurring in welded steels with high hardenability. After welding, cracking typically occurs at some temperature below 93 °C (366 K), immediately upon cooling or after a period of several hours. The time for cracking depends on the type of steel, the magnitude of the welding stresses, the hydrogen content of the steel weld and the heat affected zone (HAZ), and service temperature. Weld metal cracking, seldom occurs when the yield strength is below about 90 ksi (620 MPa) and its cracking susceptibility has been reported to be proportional to the yield strength of the weld metal deposit. The resulting cold cracking problems have been termed hydrogen embrittlement, hydrogen induced cracking, cold cracking, hydrogen delayed cracking, or hydrogen assisted cracking (HAC).

Hydrogen-assisted cracking is a very common problem encountered during the fabrication of high strength steel structures. With the advances in high strength low alloy (HSLA) steel processing, cracking has moved from the HAZ to the weld metal. The susceptibility to hydrogen-assisted cracking has been primarily related to the steel composition, microstructure, and temperature.

For better understanding of HAC for steel weldments, two classifications of hydrogen must be considered. Diffusible hydrogen is the mobile hydrogen that is available for diffusion to the tri-axial stress sites and is considered to potentially harmful for HAC. The residual hydrogen is the hydrogen that is trapped at specific sites in the microstructure, preventing its transport. The prevention or control of diffusible hydrogen in the weld metal may reduce the susceptibility to hydrogen cracking.

Current preventive measures such as pre- and/or post-weld heat treatment, proper electrode selection and handling, and edge preparation have been used to minimize the hydrogen concentration and stress level. Through these practices, HSLA steel welds can maintain acceptable levels of diffusible hydrogen content as low as two milliliters of hydrogen per 100 grams of weld deposit. However, these practices require much effort, time, and expense.

1.2.2 Hydrogen Management in Steel Weldments

ARO sponsored research at CSM has offered new approaches to hydrogen management in steel weldments through the use of hydrogen trapping additions. The investigation of hydrogen trapping and welding parameters for a gas metal arc welding process using a hydrogen trap containing metal-cored electrodes was performed on high strength low alloy (HSLA) steel. The purpose of this study was to reduce and control the diffusible hydrogen content in the weld deposit and to further our understanding of the hydrogen trap behavior in welds, so that a practice of using weld metal traps to control the diffusible hydrogen content and its distribution can be developed resulting in a new generation of welding consumables for defense related high strength steels. Effective control of weld diffusible hydrogen content has been achieved with the use of irreversible hydrogen traps in higher strength steel weld deposits. The benefit of yttrium addition as an irreversible hydrogen trap in the weld metal was observed by decreasing the diffusible hydrogen content in the weld metal to appreciable levels around one to two milliliter of hydrogen per 100 g weld deposit. In addition, the weld metal diffusible hydrogen content is affected by variations in welding parameters including voltage, current, travel speed, and oxygen contents, which also affects the heat input and metal transfer mode across the arc. The spray mode promotes more efficient transfer of yttrium to the weld deposit, resulting in less diffusible hydrogen, less than 1 ml/100g weld deposit, and higher trapped hydrogen in the weld deposit compared to the globular transfer mode. Much of the hydrogen trapping research was performed in the previous contract period. Hydrogen trapping research was drawn to a successful conclusion during the present contract period. A major review of hydrogen trapping in steel weld metal was invited and published in the International Journal of Materials Review [7].

1.2.3 Beneficial Opportunities from Hydrogen

An ARO sponsored investigation has demonstrated that hydrogen can increase the plasticity of hydrogen charged 2 1/4 Cr-1Mo steel during high temperature forming. This enhanced formability is strongly dependent upon the amount of hydrogen, as well as the strain rate. This enhanced formability can be explained by the difference in the mobility of dislocations. The positive effects of hydrogen on the plasticity at higher temperatures and the possible mechanisms which led to the distinct decrease in the compressive stress of 2 1/4 Cr-1Mo steel and becoming comparable to iron are discussed in detail; taking into account flow and recovery as well as dynamic recrystallization [8].
A collaborative research effort between CSM, Dortmund University (Germany) and Ben Gurion University of Negev (Israel) also demonstrated similar advantages of hydrogen enhanced plasticity of Ti-Nb alloys.

1.3 Nitrogen Behavior in Metal and Alloys

When nitrogen is used as an alloying element, nitrogen enters the metal matrix as an interstitial atom where it is introduced into spaces or sites between lattice positions in the host metal. In the Fe-N matrix, the tetrahedral and octahedral sites provide interstitial sites for nitrogen. When the nitrogen atom occupies a tetrahedral site it causes displacement of four neighboring atoms, while the occupation of an octahedral site requires the displacement of six neighboring atoms. In the face-centered cubic lattice, the radius of the metal atom is $r=a/2.28284$ where a, is the lattice parameter [9].

The number of occupied interstitial sites in the metal lattice is much lower than the number of available interstitial sites. When nitrogen occupies an interstitial void, the nearest neighbor atoms are shifted, thus causing a displacement field or lattice strain. The superposition of these long-range displacement fields leads to a strained expansion in the entire lattice making it more difficult for neighboring interstitial sites to become occupied, thus resulting in a decrease in the nitrogen solubility to a level lower than is geometrically possible [9].

In steel, nitrogen atoms prefer to occupy only octahedral sites both in the α-phase and γ-phase. The austenite phase has higher solubility, which is due to larger site sizes. Nitrogen prefers to occupy the octahedral voids because the occupation of a tetrahedral void requires outward displacement of all four neighboring iron atoms, whereas the irregular octahedral site can be occupied with the displacement of only two iron atoms parallel to the cube edge. This displacement of the iron atoms leads to lengthening of the lattice in the direction causing the lattice distortion or residual strain resulting in a change in the amount of *d*-orbital overlap. The amount of d-orbital overlap effects the electron concentration in the d-band by the Pauli-exclusion principle and thus altering the shape of the d-band. A change in the shape of the *d*-band results in a signification change in the effective electron mass and thus a change in the thermoelectric power coefficient (TEP) coefficient.

Strain in the crystal lattice is not only caused by the ratio of atomic sizes, but strain is also due the nature of chemical binding between the metal and the interstitial atoms. The chemical binding occurs by nitrogen contribution of electrons to the 3d-band of the host metal. Therefore, the solubility of nitrogen relies on the availability of space for their p-electrons to be donated to the d-band. Nitrogen solubility decreases rapidly as the d-band in the metal host becomes increasingly full. This donor model is not likely workable on the alloys made up of transition elements on the right side of the transition metal series where the heat of mixing is negative, but of a small magnitude [9].

1.3.1 Effect of Nitrogen Solubility on Weld Metal Nitrogen Content

For austenitic iron, nitrogen solubility limit is approximately less than 0.03 wt. pct. as shown in Figure 2. Changes in nitrogen solubility occur due to alteration of alloy composition, crystal structure, temperature, and N_2 melt pressure. Alloying additions such as chromium, manganese, and molybdenum increase the nitrogen solubility while nickel, silicon, and carbon decrease the nitrogen solubility. German alloy 1.4565 has a nitrogen content of 0.458 wt. pct. prior to welding, which is beyond the saturation limit of face-centered cubic iron. However, alloying additions can either increase or decrease the nitrogen solubility. If the solubility limit is exceeded, the formation of brittle nitrides can possibly occur.

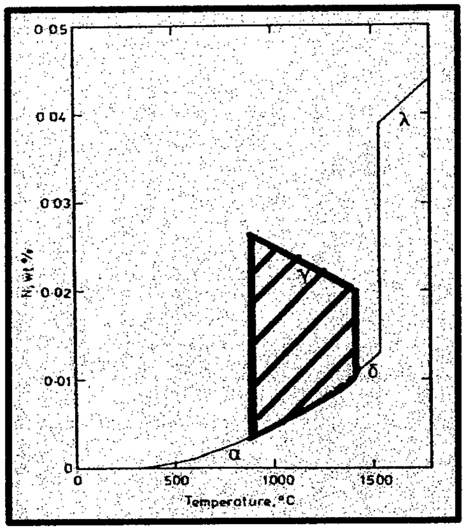

Figure 2. Nitrogen content versus temperature of steel with the austenitic region highlighted in red.

The nitrogen-alloy equilibrium can be best understood using the PCT (pressure-composition-temperature) diagram determined by Sieverts' analytical set-up. Figure 3 illustrates a schematic of such a diagram. PCT diagrams, which are commonly used for assisting hydrogen storage capacity in alloys, should be applied to the new nitrogen strengthened austenitic stainless steels to establish a clear understanding of what it means to alloy with nitrogen.

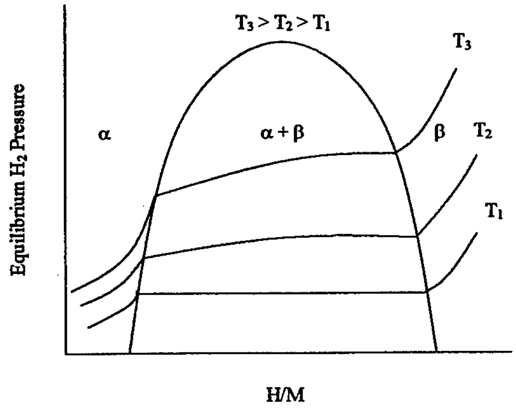

Figure 3: Schematic pressure-composition-temperature diagram for nitrogen.

During welding, the solubility of nitrogen is not only affected by alloy additions, but also by weld parameters. Weld parameters such as the welding current and the weld travel speed both affect the solubility of nitrogen in weld metal. With increasing current, the nitrogen concentration decreases and with increasing travel speed the nitrogen concentration increases. Nitrogen concentration can be influenced by weld parameters, which affect the size of the weld bead because as the area of the weld pool increases, the nitrogen concentration decreases. According to Kuwana, et al, for stainless steel, the nitrogen concentration almost doubles when the weld travel speed increased from 50 to 300 mm/min. The behavior is modeled as weld pool dwell time and size affects the nitrogen concentration for these high nitrogen alloys, which depend on nitrogen strengthening. Thus careful management of nitrogen to achieve the desired mechanical properties needs to be established and thoroughly understood.

1.3.2 Beneficial Effects of Nitrogen

Nitrogen is used as a solid solution alloying element for strength and corrosion resistance. Nitrogen can also be used to form carbo-nitrides as another strengthening mechanism in high strength low alloy steels. The higher the nitrogen concentration, the higher the tensile strength.

The addition of nitrogen to austenitic stainless steels significantly improves the strength and the pitting resistance of the alloy and it may also improve the cryogenic toughness. Austenitic alloys may contain high levels of manganese resulting in an increase in nitrogen solubility. Nitrogen is also a valuable substitution for nickel being twice powerful as an austenite stabilizer at a much lower price. Nitrogen strengthened stainless steel offers non-magnetic structures for military use.

1.3.3 Detrimental Effects of Nitrogen

In welding of nitrogen strengthened stainless steels it is essential to avoid nitrogen losses, weld defects, and nitride precipitation, which could result in loss of corrosion resistance as well as mechanical properties. The influence of nitrogen in stainless steel welds is a complex and less studied phenomena than nitrogen in base metal. The two most serious problems associated in the welding of high nitrogen strengthened stainless steels are solidification cracking in the weld metal and liquation cracking in the heat-affected zone. Porosity is another problem associated with welding of high nitrogen stainless steels. Porosity in welds is attributed to nitrogen gas that escapes as porosity due to a difference in nitrogen gas solubility between molten and solid metals. Pore formation initiates in the interdendritic region, the same location as hot cracking. Existing hot cracking models suggest hot cracks initiate on interdendritic pores.

In welding of austenitic stainless steels, which can normally accommodate significantly high levels of nitrogen in the metal matrix, nitrogen desorption to the arc atmosphere occurs leading to a decrease in weld metal nitrogen content upon solidification. The welding thermal experience can also promote nitride formation in the heat-affected zone also causing a reduction in nitrogen enhanced solid solution strengthening. A decrease in nitrogen content can be detrimental to the life of the weld, therefore a thermoelectric power surface-probe measuring scheme, which can conveniently determine weld nitrogen concentration, would significantly improve ability to guarantee integrity.

2.0 SUMMARY OF THE IMPORTANT RESULTS

This section discuss the summary of important work completed during this contract. This work includes a thermodynamic interpretation of thermoelectric power to hydrogen content and the use of thermoelectric power to assess nitrogen content in alloys. Work also includes the assessment of hydrogen content in structural alloys, hydrogen storage capabilities, hydrogen as an alloying addition, irreversible hydrogen traps, and hydrogen-assisted forming.

2.1 Thermoelectric Power Coefficient for Sensing of Hydrogen in Alloys

Smart materials offer a solution to increase the reliability of technical systems and structures. Smart materials are materials that produce a measurable response with small stimuli allowing assessment of material properties that can be correlated to structural integrity criteria. With the application of sound engineering, solid state physics concepts, and appropriate property characterization and correlation, most structural alloys automatically become smart materials with the use of either active and/or passive electronic property sensors. The electronic materials industry has developed advanced analytical instrumentation for the rapid and accurate electronic property measurements, which have lead their research and assessed their product quality. It is now advantageous to use electronic property measurements to measure the electronic state of structural alloys to assess their stability and tendency for damage before significant defects arise. ARO funded a DURIP equipment grant for electronic measuring equipment for a CSM laboratory to measure electronic properties of structural alloys which has been significant contribution to research efforts.

The thermoelectric power (TEP) analysis was used to measure the potential response to a small perturbation in temperature between two locations; This perturbation causes an electron flow resulting in a measurable potential difference. This cause and effect behavior is assessed by the TEP coefficient (the Seebeck coefficient) between the differential voltage and differential temperature across these two locations. This coefficient provides a wealth of information about the alloy. The TEP coefficient is a function of the electronic scattering behavior, the electron concentration, and the effective mass of the electron in this alloy. All three of these factors are influenced by the solute content, lattice strain, microstructural changes, material processing and time-dependent phase transformation (including aging). The TEP coefficient is a valued property for microstructural assessment. Because alloy microstructure correlates directly to properties, the thermoelectric power coefficient is a rapid and effective way to assess alloy aging and microstructural changes that can potentially lead to significant defects and possible structural failure.

In metallic alloys, the value and the sign of the TEP coefficient depends on the electronic density of states features in the vicinity of the Fermi energy level and is dependent on the effective mass tensor, density of electronic states, dominating scattering mechanism, etc. In turn, the Fermi energy value (Fermi surface in the k-space) changes with electronic filling in the conduction band due to the electron donation by hydrogen atoms. For example, for a parabolic band and high degeneracy of the electron gas, the resulting TEP coefficient, α, is related to the free electron theory through the following expression, which holds for high carrier concentrations and $(E_f\text{-}E_o)/kT > 5$:

$$\alpha = \left(\pm\frac{k}{e}\right)(27.1)\left(r+\frac{3}{2}\right)\left(\frac{m_e}{h^2}\right)\left(kTn^{*\left(-\frac{2}{3}\right)}\right) \qquad [1]$$

where r is the scattering parameter determined by the dominating scattering mechanism, h is Planck's constant, k is Boltzmann's constant, n^* is the free electron concentration, and m_e is the effective mass. From the free electron model, the electron concentration is directly related to the Fermi energy. The effective mass describes the rate of filling of the energy states in k space at the Fermi energy level with increasing electron concentration. The effective mass can be described as:

$$m_e = \hbar^2\left(\frac{d^2E}{dk^2}\right)^{-1} \qquad [2]$$

where k is the wave vector. The effective mass, m_e, describes the shape of the *s*, *p*, and *d* bands that are in contact with the Fermi energy level. The shape of the bands at the contact position offers a characteristic signature of the state of the alloy that can be measured and assessed for lattice strain and phase stability.

2.1.1 Thermodynamic Interpretation of TEP Correlation to Hydrogen Content

Thermoelectric power involves the generation of the Seebeck electromotive force, dV, under an applied temperature difference, dT. Thermodynamically the TEP coefficient can be related to external work (similar to the electrochemical equation), as shown in the following equations:

$$dG = VdP - SdT + \left(\frac{\partial G}{\partial n_H}\right)dn_H - dW_{ext} \qquad [3]$$

where G is the Gibbs free energy, V is the volume, P is the pressure, S is the entropy (lattice effects), T is the temperature, n_H is the mole of hydrogen, and W_{ext} is the external work. With dn moles of transported electrons and Faraday's constant, F, the chemical potential and magnitude of the work of the charge carried by one mole of electrons under the temperature gradient is represented by:

$$\mu_H = \left(\frac{\partial G}{\partial n}\right)_{P,T} \qquad dW_{ext} = -nFdV \qquad [4]$$

By substituting these terms into equation 3, the following equation can be obtained:

$$dG = VdP - SdT + \mu_H dn_H - nFdV \qquad [5]$$

When the system is in reversible equilibrium, such that $dG = 0$ and $dP = 0$,and $dV = \alpha dT$, then equation 5 becomes:

$$0 = -SdT + \mu_H dn_H - nF\alpha dT \qquad [6]$$

where α is the Seebeck Coefficient. Equation 6 can be converted into equation 7:

$$\alpha = \frac{S}{nF} - \frac{\mu_H dn_H}{nFdT} \qquad [7]$$

For the reaction of hydrogen 2H → H$_2$; then $\mu = \mu_{H_0} + RT\ln\frac{P_{H_2}}{[H]^2}$; resulting in:

$$\alpha = \frac{S}{nF} - \left(\mu_{H_0} + RT\ln\frac{P_{H_2}}{[H]^2}\right)\left(\frac{dn_H}{nFdT}\right) \qquad [9]$$

For diffusible hydrogen $n = dn_H$ and hydrogen gives its electron to *d*-band, such that

$$DT = \Delta T \qquad \text{and} \qquad \alpha = \frac{S}{nF} - \left(\mu_{H_0} + RT\ln\frac{P_{H_2}}{[H]^2}\right)\left(\frac{1}{F\Delta T}\right) \qquad [10]$$

where ΔT is the applied temperature difference between contact probes.

A schematic diagram of the TEP coefficient measurement setups used for this study are shown in Figure 4 (a) and (b). The temperature difference is measured between two reference blocks or probes. The TEP coefficient is the potential difference between the copper and the specimen divided by the temperature difference between the copper blocks (probes). The TEP coefficient of the alloy material, S$_a$, can be determined from measurements as:

$$\alpha_a = \frac{V}{\Delta T} + \alpha_{Cu} \qquad [11]$$

where *V* is the Seebeck voltage measured between probes, *ΔT* is the temperature difference, and α_{Cu} is the well-calibrated Seebeck coefficient for copper. One of the copper blocks (probe) was maintained at room temperature and the other one at a temperature higher by 10 °C.

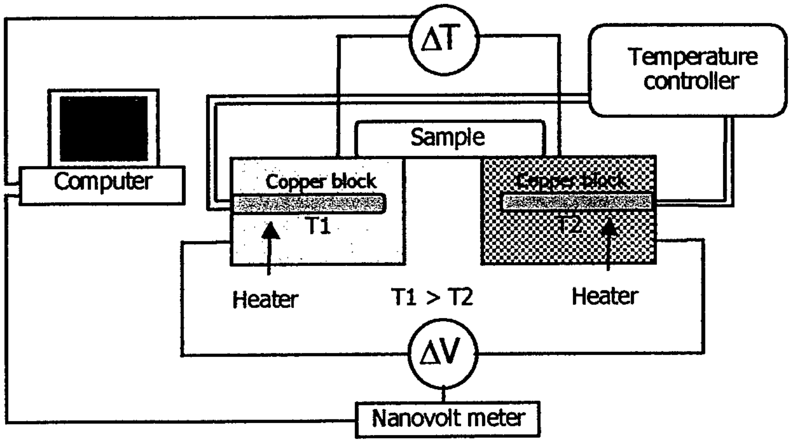

(a)

(b)

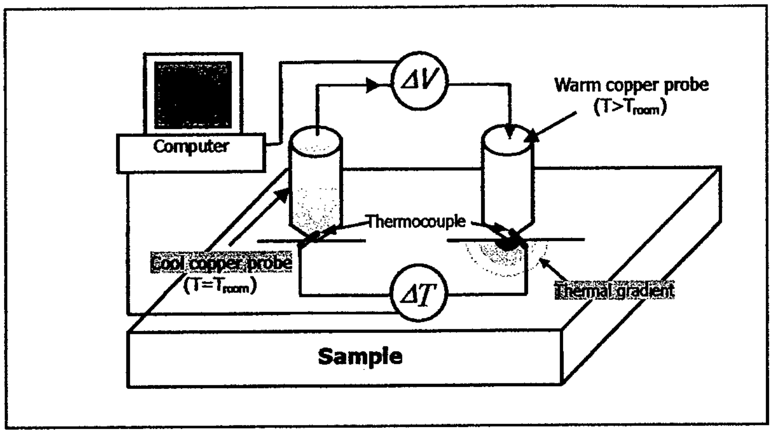

Figure 4. Schematic diagram of the TEP coefficient measurement system: Advanced TEP coefficient measurement with nano-voltmeter and temperature controller for both copper probes. (a) Illustrates the use of temperature controlled blocks and (b) illustrates use of temperature controlled copper probes.

2.1.2 Assessment of Hydrogen Content in Structural Alloys

Demonstration on Monel 500 and Invar

In this investigation the effective use of TEP coefficient measurements to determine the diffusible hydrogen content in various alloys was evaluated. Hydrogen charged Monel K-500 and Invar (64-36 wt. pct. Fe-Ni) are described. Chemical compositions for these alloys are summarized in Table 1. This approach of using surface contact electronic property measurements to assess hydrogen content in an alloy is rapid and non-destructive.

Table1. Chemical composition by weight percent for Invar and Monel K-500 alloys.

Alloy	C	Si	Mn	P	S	Cr	Ni
Invar	0.004	0.1	0.05	0.005	0.004	0.2	32.0
Monel K-500	0.13	0.25	0.75	-	0.01	0.15	66.5

Alloy	Nb	Mo	Al	Ti	Cu	Co	Fe
Invar	-	-	-	-	-	5.5	Bal
Monel K-500	-	-	2.75	0.60	Bal	-	1.0

To charge the hydrogen into the specimens, a high pressure gaseous hydrogen and high temperature charging system was built and used. Various combinations of temperature, pressure, and cooling rate control can be achieved with this charging system. Once hydrogen charging was completed, the hydrogen content was measured using a LECO RH-404 hydrogen determinator.

TEP coefficient measurements were examined for Monel K-500. Monel K-500 is an age hardenable nickel-copper alloy with excellent corrosion resistance, strength and hardness. It has been found that hydrogen assisted cracking occurs in Monel K-500 during naval service, especially in parts experiencing a cathodic corrosion protection. It has been recognized that a convenient and rapid non-destructive hydrogen content measurement technique is desirable to determine the critical load. The hydrogen content (or TEP measurement) was compared to a critical unacceptable value.

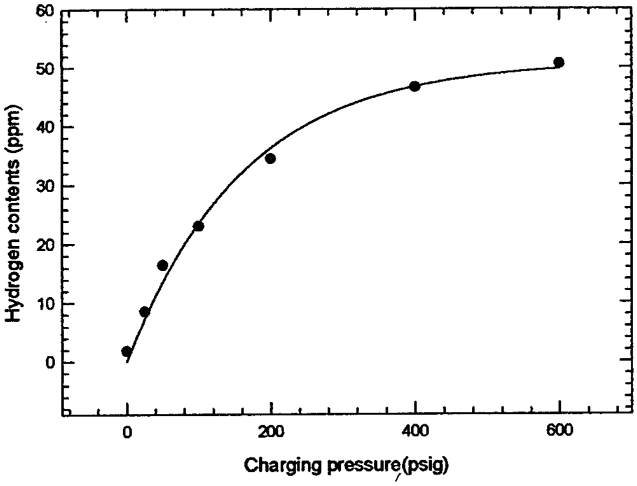

Figure 5. The hydrogen content as measured by the hydrogen determinator for each charged Monel K-500 specimens. Charging was conducted at 400 °C and 48 hours, followed by water quenching.

All of the Monel K-500 specimens were annealed at 1073 K (800 °C) for ten hours in an argon atmosphere to achieve an identical initial condition. The charging was performed at five different pressure levels (25, 50, 200, 400, and 600 psig) for 48 hrs at 673 K (400 °C) to obtain different hydrogen contents for each specimen. The hydrogen content varied from just over 2 ppm for an annealed specimen up to 50 ppm for a 600 psig charged specimen. The results for total hydrogen content for each specimen is shown in Figure 5. Hydrogen contents increased steeply until reaching the charging pressure of 400 psig and then gradually increased up to 600 psig. The parabolic curve suggests that hydrogen content as a function of charging pressure follows Sieverts' law for hydrogen absorption in an equilibrium condition. The absorption of pressured hydrogen into the specimen can be described using Sieverts' Law:

$$H = K \exp\left(\frac{-\Delta G}{RT}\right)\sqrt{P_{H_2}} \qquad [12]$$

where H is the amount of absorbed hydrogen, ΔG is the standard free energy, K is a temperature-dependent constant, R is the gas constant, T is the absolute temperature and P_{H_2} is the partial pressure of hydrogen in a hydrogen charging reactor. TEP measurements were made on Monel K500 charged to different levels of hydrogen content as seen in Figure 6. With increasing hydrogen content, the TEP coefficient first increased and then leveled off at 10 ppm hydrogen. This behavior suggests that at 10 ppm a new phase was formed and the leveled region corresponds to a two-phase region.

These results suggest that there are microstructural transformations occurring during hydrogen charging. It has also been observed that TEP coefficient is very sensitive to microstructural changes such as precipitation phenomena or solute concentration changes. Therefore, it is proposed that microstructural changes occurred for Monel K-500 specimens during charging. One hypothesis is the formation ε-martensite due to hydrogen charging into specimens. The ε-martensite formation occurs in austenitic stainless steels and has been observed by numerous researchers. Rozenak *et al.* [10] found hydrogen-induced phase transformation of the γ-FCC phase to the ε-HCP martensitic phase in an austenitic stainless steel. When hydrogen is introduced in austenitic microstructure, it decreases the stacking fault energy (SFE), which would change the array of stacking to "ABAB" (HCP structure). This effect results in hydrogen-induced ε-HCP precipitation, and changes the TEP coefficient for low hydrogen content specimens. Other evidence for phase instability with hydrogen charging was found by Uwakweh *et al.* for cathodically charged stainless steels [11].

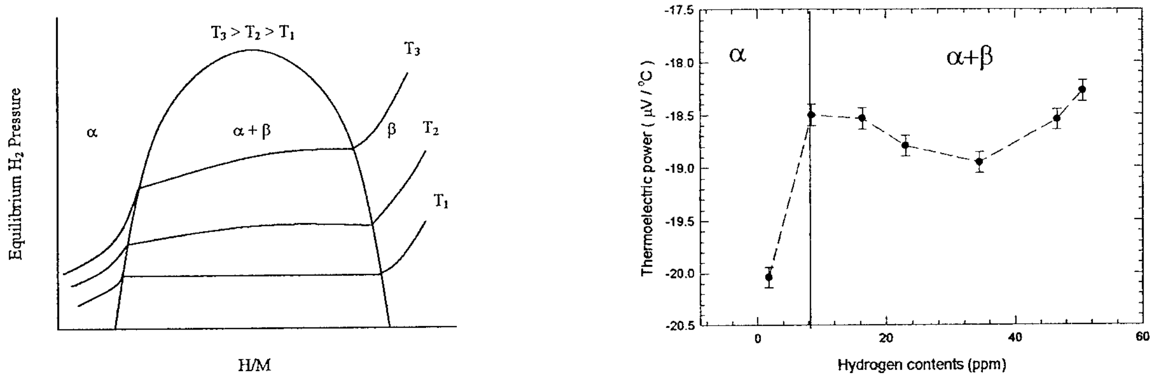

Figure 6. Correlation of TEP coefficient with PCT diagram for hydrgoen. The clear separation between the a and a+b region can be seen.

With regular x-ray diffraction analysis, no significant difference between the x-ray diffractograms of the hydrogen charged specimens was observed. All specimens gave reflections of the α-phase, with a shift towards higher angles as shown in Figure 7a. However, if the amount of the phase formed by hydrogen charging is very small, it can be detected only by very slow scan. It was decided to perform a long scan on the 200 psig hydrogen charged specimen (34 ppm hydrogen content), in which the detection of small phases was most likely. In the diffractogram with a slow scan (step size = 0.04 deg, 40 sec per step) obtained small peaks clearly seen in Figure 7b. Hence, the hydrogen charging resulted in a minor phase transformation.

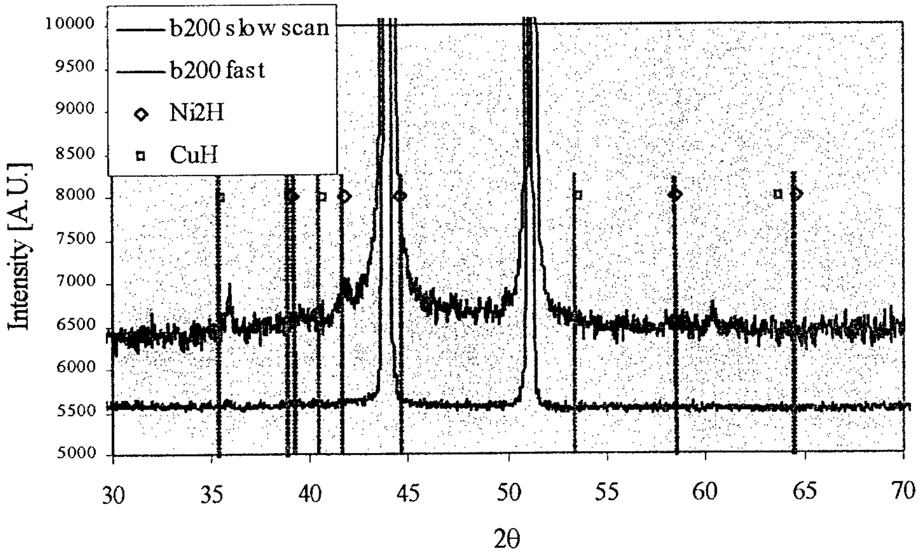

Figure 7. XRD diffractograms of a) fast scan and b) slow scan for the hydrogen charged Monel K-500. Charging condition: 200 psig, 400 °C, and 48 hours.

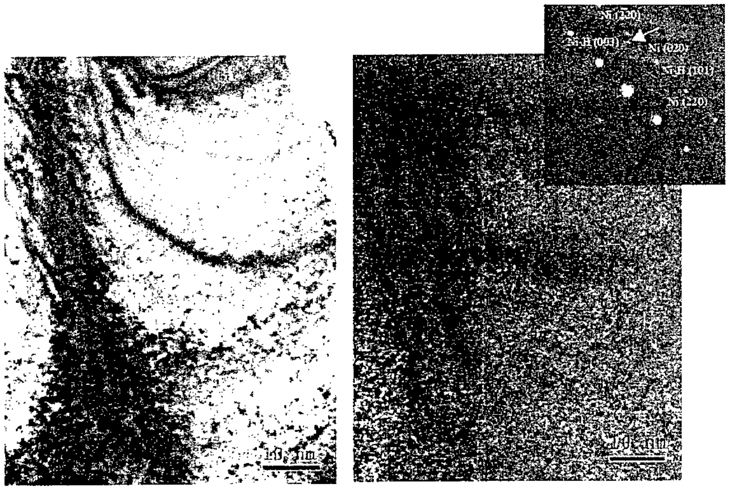

Figure 8. TEM images of 900 psig hydrogen charged specimen revealed nano- sized participates dispersed in the Ni matrix.

As shown in Figure 7b, the small peaks, which appeared in the slow scan, were found to correspond to either Ni_2H or CuH phase. The ε-martensite phase was not observed according to X-ray diffraction results. Therefore, X-ray diffraction analysis suggests that hydrogen charging begins to form a hydride phase and deviation in the TEP coefficient curve can be explained with a hydride phase formation.

TEM investigation of the 900 psig hydrogen charged specimen revealed nano sized participates dispersed in the Ni matrix (Fig. 8a). In a selected area electron diffraction (SAED) reflections of the Ni_2H phase were identified (see inset in Fig. 8). The nano-sized participates were consistent with the Ni_2H phase in the dark field image taken from one of the Ni_2H reflections (marked by arrow).

X-ray diffraction analysis suggests that hydrogen charging starts to form a Ni-hydride phase and deviation in the TEP coefficient curve can be explained with a PCT (pressure composition isotherm) with higher hydrogen content also suggested in Figure 6. The PCT diagram can divided into three regions, first (a), second (α+β), and third (β) in the first region, hydrogen is in solid solution and is called the alpha phase (α). The reaction of hydrogen absorbed in this region is $1/2\ H_2(g) \rightarrow H(M)$. The second region is two-phase region(α+β), the so called plateau region. In this region, there is the coexistence of solid solution and hydride phase. In the third region, hydrogen is in the form of a metal hydride and is called the beta phase (β) As hydrogen is charged from 50 psig and higher pressure at 400°C, the Ni_2H phase starts to form, which corresponds to the second region (α+β) of the PCT diagram as shown in Figure 6. However, an actual PCT diagram for Monel K-500 alloy is not known.

2.1.3. Assessment of Hydrogen Storage Capability

An investigation was performed that has very effectively used physical chemistry, modern physics, and microstructural science to bring new insight into the hydrogen behavior in AB2 and AB5 hydrogen storage materials [12]. This effort correlated the results from pressure-composition-temperature diagrams (PCT diagrams), the classical chemistry approach to characterize these materials, with thermoelectric power coefficient and magnetization analyses to offer a rapid and accurate assessment of a materials hydrogen storage capability through the use electronic property measurements. The ability to assess effective reversible hydrogen charging and discharging was further evaluated by correlating electronic property measurements with microstructural analysis. Microstructural analysis identified the proper microstructural features offering fast hydrogen transport and significant hydrogen storage. The use of these advanced analytical tools allows for a more rapid method to select new hydrogen storage materials.

AB_5 Alloy Assessment

Experimental AB_5 and AB_2 alloys of composition give in Table 2 were evaluated using TEP measurements to determine the hydrogen content in the material.

Table 2: Chemical composition of AB_2 and AB_5 Alloys

Alloy	Type	A						B							B/A Ratio
		Mg	Zr	Ti	La	Nd	Ce	Ni	Mn	Cr	V	Fe	Al	Co	
1	AB_5	0.6			7.7		8.1	71.2	12.0				0.4		5.1
2	AB_5				8.3	8.3		59.2	6.7				5.0	12.5	5.0
3	AB_2		19.0	8.1				29.2	16.9	20.7	8.4				1.8
4	AB_2		30.0	3.3						20.0		46.7			2.0

Alloy 1, (La-Ce)(Ni-Mn)$_5$, and Alloy 2, (La-Nd)(Ni-Co-Mn)$_5$, are of type AB_5. Figures 9 and 10 show the hydrogen desorption curves determined by gas chromatography. The initial hydrogen charges were 2.23 and 1.83 per formula unit. Desorption of diffusible (protonic) hydrogen, which most likely is present in the alpha phase, occurs at about 220 °C and 110°C, respectively. The release of bound hydrogen at temperatures above 600 °C is indicative of hydride decomposition in Alloy 1. Both the low-temperature desorption and the absence of bound hydrogen would make Alloy 2 a good candidate for battery applications.

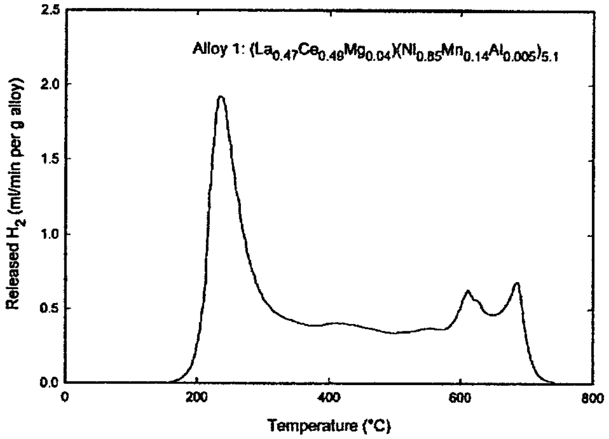

Figure 9. Hydrogen desorption curve for Alloy 1 hydride as a function of temperature.

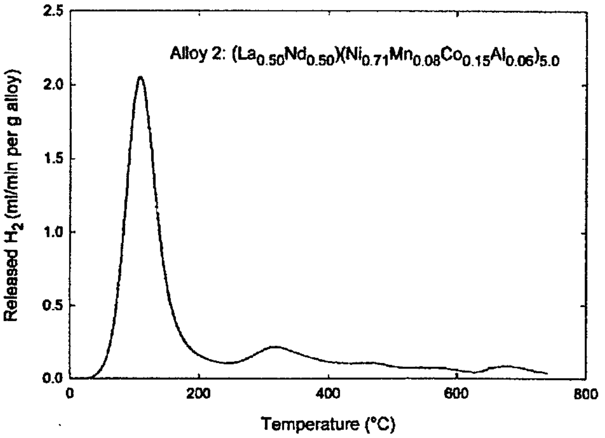

Figure 10. Hydrogen desorption curve for Alloy 2 hydride as a function of temperature.

The magnetization curves and the technical saturation magnetization as a function of hydrogen contents for Alloy 1 are shown in Figures 11 and 12. (To convert magnetic field from units of Tesla to units of ampere per meter, multiply by 107/41t. To convert magnetic field from SI units of Tesla to CGS units of gauss, multiply by 104.) The technical saturation magnetization is the magnetization axis intercept of a line fitted to the high field part of the curve of magnetization as a function of field. An increase in diffusible hydrogen decreases the magnetization of Alloy 1. The DFEC number for Alloy 1 is calculated as 6.51, whereas the number of electrons required to half-fill the *d*- and *f*-shells is 5.47. The reduction of magnetic moment results from electrons donated by the hydrogen atoms pairing with the unpaired electrons in the host metal.

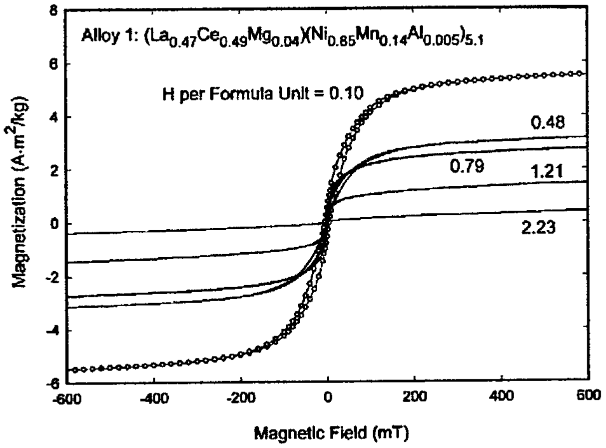

Figure 11. Magnetization versus field for Alloy 1.

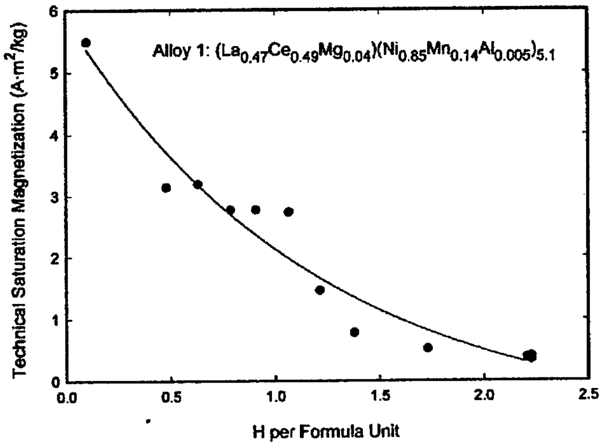

Figure 12. Technical saturation magnetization as a function of hydrogen content for Alloy 1.

As hydrogen content increases, magnetization and hysteresis decrease. For Alloy 2, as a function of hydrogen content, Figure 13 shows the magnetization curves and Figure 14 shows the initial susceptibility near zero field (not corrected for demagnetizing factor) and high field susceptibility. Initially, the susceptibilities decrease as hydrogen increases, but then increase after the ratio of hydrogen to metal is 1. The susceptibilities decrease again when the hydrogen-to-metal ratio is greater than 2. The computed DFEC number of Alloy 2 is 6.48, also above the number of electrons to half fill the *d*- and *f*-band, 5.33. Therefore, a decrease in susceptibility is expected. The difference in the magnetic behavior between Alloys 1 and 2 may depend on the details of the actual band structure of the alloys.

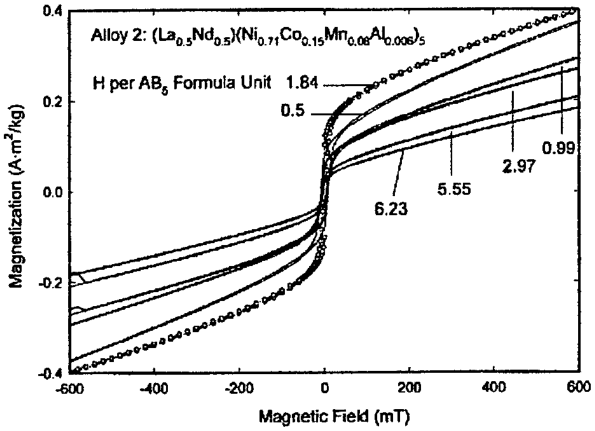

Figure 13. Magnetization versus field as a function of hydrogen content for Alloy 2.

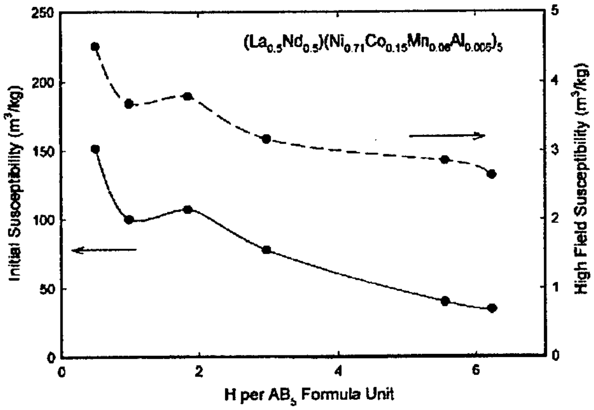

Figure 14. Initial and high field susceptibilities as functions of hydrogen content in Alloy 2.

The room temperature Seebeck coefficients and PCT isotherm of Alloy 2 are shown in Figure 15. The Seebeck coefficient of this alloy increases with an increase in hydrogen content until it reaches a plateau region, in which the two-phase reaction occurs, at a hydrogen content per formula unit of about 1, and increases again at the transition from the two-phase region to the single-phase hydride region. In the first stage, each hydrogen atom provides an electron to the host material, which changes the Fermi energy level of the material. In the plateau region, lattice expansion occurs as the bound hydrogen forms a hydride, and the added electrons from the hydrogen have less of an effect on the Fermi energy.

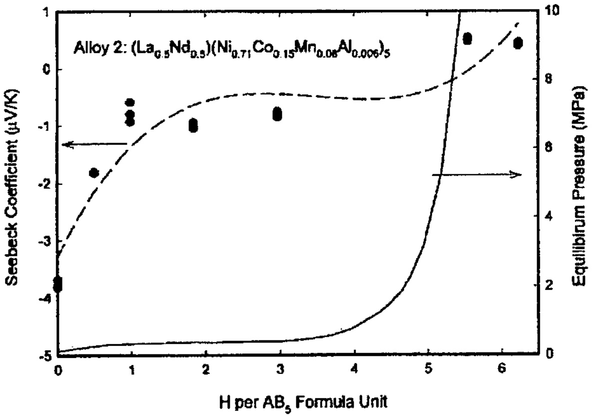

Figure 15. The thermoelectric power (Seebeck coefficient) at 25 °C and the PCT diagram at 75 °C of Alloy 2 as functions of hydrogen content.

AB_2 Alloys Assessment

Unlike Alloys 1 and 2, Alloy 3, which is AB_2 type, has a main hydrogen desorption peak at 680 DC, as shown in Figure 16. The initial hydrogen charge was 0.91 per formula unit. This result indicates that most of the hydrogen in Alloy 3 is stored as bound hydrogen, with a little amount of diffusible hydrogen indicated by peaks at lower temperature. In contrast, the hydrogen desorption curve of Alloy 4, shown in Figure 17, shows a main peak at 220 DC, which is in the diffusible hydrogen range. The initial hydrogen charge was 4.10 per formula unit. The relatively large amount of released hydrogen per gram of Alloy 4 is due to its low molecular weight and its large initial hydrogen content from gas-phase charging.

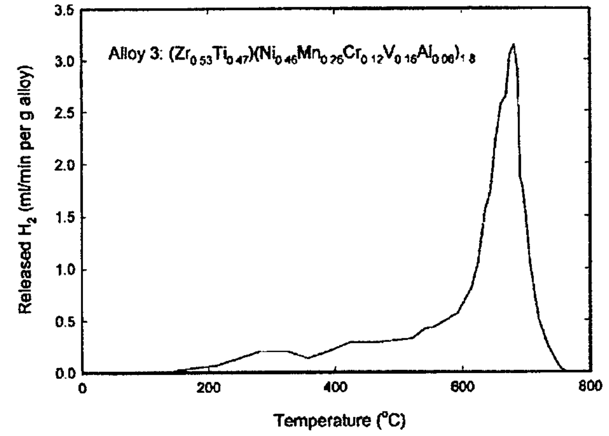

Figure 16. Hydrogen desorption curve for Alloy 3 hydride indicating the release of hydrogen only at a high temperature of about 680 °C

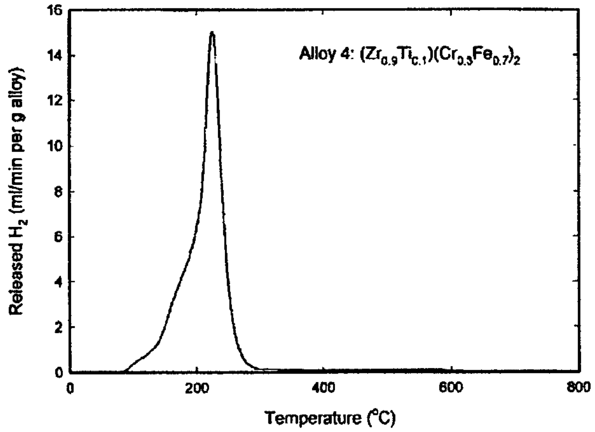

Figure 17. Hydrogen desorption curve for Alloy 4 hydride indicating the release of hydrogen at 220 °C

Magnetization curves and the initial susceptibilities of Alloys 3 and 4 are shown in Figures 18, 19, 20, and 21. Both the change in hydrogen content and the change in susceptibility of Alloy 3 are relatively small compared with Alloy 4. The calculated DEC number of Alloy 3 is 4.23, which is less than the number of electrons required to occupy a half-shell. Therefore, if hydrogen gives additional electrons only to the *d-shell,* the initial susceptibility should increase with the amount of hydrogen. However, the initial susceptibility curve for Alloy 3 shows that hydrogen has almost no effect on the initial susceptibility (Figure 19). Since Figure 16 shows that Alloy 3 holds hydrogen as *bound* hydrogen, the transfer of an electron from the host metal and the formation of the hydride bonding band may dominate and not affect the magnetic moment. (A reduction of the Fermi energy during hydride formation was reported for $LaNi_5$ [13].)

On the other hand, the initial susceptibility for Alloy 4 *increases* with diffusible hydrogen (Figure 21). The computed DEC number of Alloy 4 is 4.27, also less than the number of electrons required to occupy a half-shell. Thus, it seems that electrons from diffusible hydrogen enter the conduction band and increase the magnetic susceptibility.

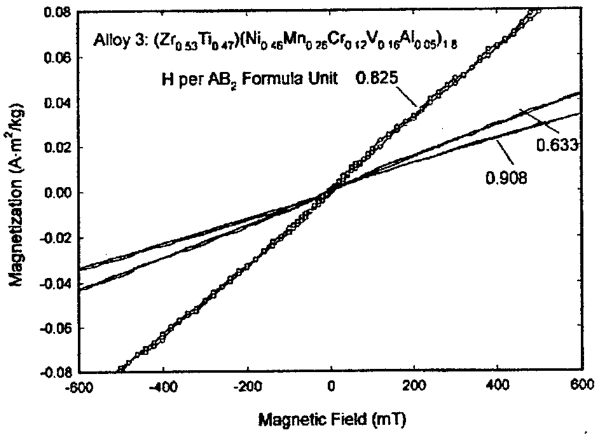

Figure 18. Magnetization as a function of applied field as a function of hydrogen content in Alloy 3.

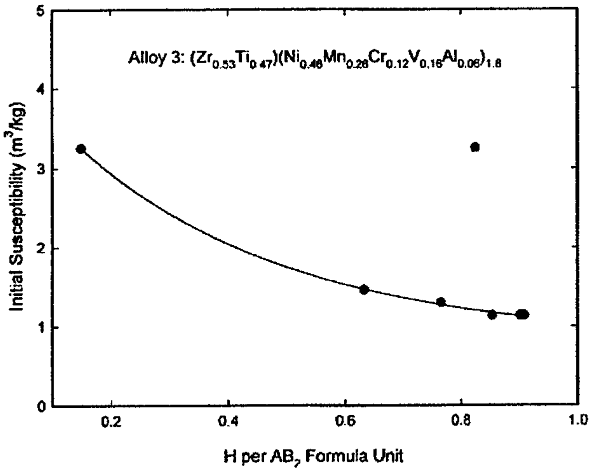

Figure 19. Initial susceptibility of Alloy 3 indicating no significant change in susceptibility as hydrogen content increases. Error bars represent the random uncertainty in the magnetization curves.

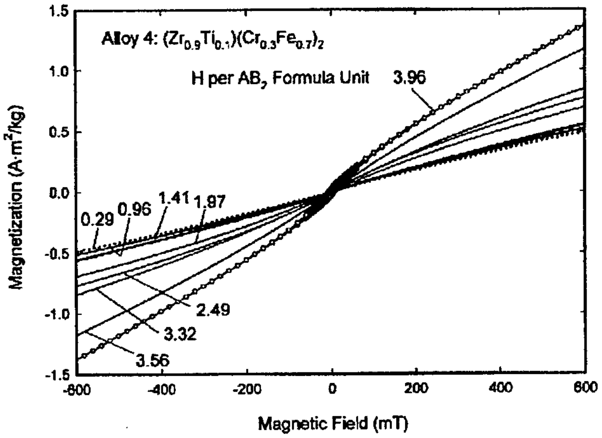

Figure 20. Magnetization as a function of applied field as a function of hydrogen content in Alloy 4.

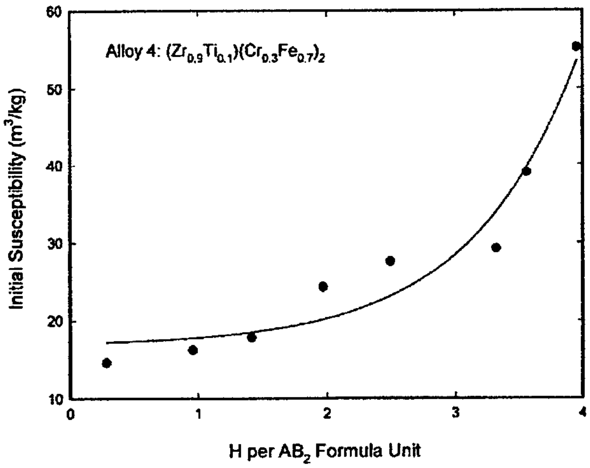

Figure 21. Initial susceptibility of Alloy 4 indicating an increase of susceptibility as hydrogen content increases.

For AB_2 alloys, the room temperature Seebeck coefficient of Alloy 3 decreases as hydrogen content increases as shown in Figure 22. Conversely, the thermoelectric power of Alloy 4 increases with hydrogen content as shown in Figure 23. The markedly different dependence of the Seebeck coefficient on hydrogen content is likely due to the different forms of hydrogen (bound hydrogen for Alloy 3 and diffusible hydrogen for Alloy 4) in the alloys.

The TEP measurement on these AB_2 and AB_5 hydrogen storage materials illustrates that a rapid electronic property measurement can replace the slow and tedious TCP measurement in the assessment of reversible hydrogen storage capability.

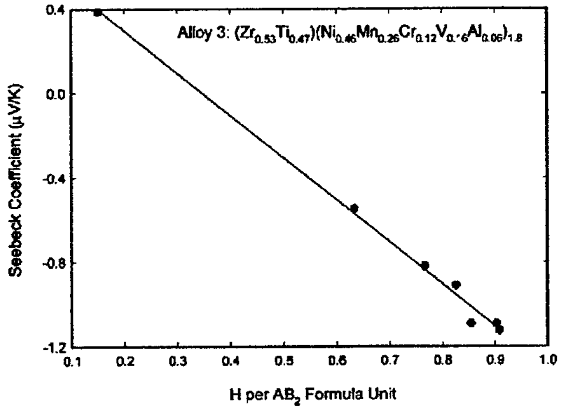

Figure 22. Room temperature Seebeck coefficient as a function of hydrogen content in Alloy 3.

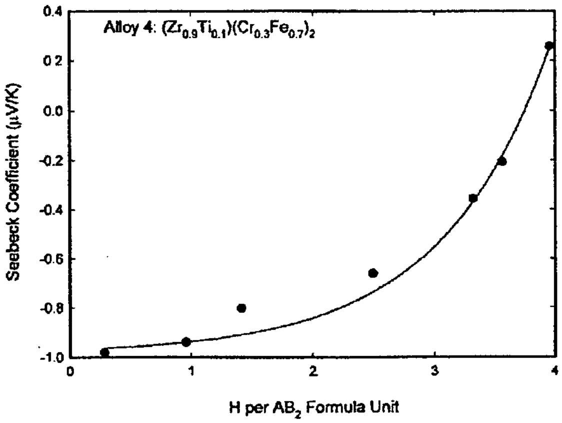

Figure 23. Room temperature Seebeck coefficient as a function of hydrogen content in Alloy 4.

2.2 Hydrogen as a Transient Alloying Addition

Use of Hydrogen as an Electron Donor to Transition Metal Alloys in the Assessment of the Influence of Small Alloy Addition on Properties

With changes in the atomic spacing as experienced in amorphous structures and the degree of order of the structure, the d-band is altered in both filling and morphology. For transition metal amorphous alloys, changes in the amount of d-orbital overlap between atoms affects the nature of exclusion principle violations and the formation of the d-band. The changes in interatomic spacing will result in changes in the d-band morphology and electron filling. Such changes can be followed by magnetic and electric property measurements. The Thermoelectric Power (TEP) coefficient, also known as the Seebeck coefficient, is a function of the electron concentration, the effective mass of the electron at the Fermi energy level, and an electron scattering factor. The last two of these factors, the effective mass and the scattering factor, respond to changes in the structural arrangement of the alloy, the tendency for phase transformations or phase stability of the alloy, the degree of alloying aging, etc.

2.2.1 Invar Investigation

Invar has the lowest thermal expansion of all metals and alloys. The mean coefficient of thermal expansion (CTE) of Invar from 20 - 100 °C is less than $1.3 \times 10^{-6}\,°C^{-1}$. It has been established that a low CTE is possible over a wide temperature range due to the interaction between phonons and magnetostriction. The TEP coefficient measurements were also conducted to observe the changes in electronic properties of Invar with hydrogen charging. In this investigation hydrogen was used as a transient alloy addition, which alters the d-band filling and shape allowing for quick assessment of Invar property changes with alloy additions of increased valence. Both hydrogen and alloying elements of higher valence than iron and nickel donate electrons to the d-band. By charging Invar to different hydrogen contents and the electronic, magnetic, and elastic property measurements. This concept of using transient alloy addition alloy stability and property assessment can be easily established without the need to prepare a large number of alloy heats to make this assessment.

Hydrogen content measurements of charged Invar specimens after 15, 30, and 60 hours were conducted at a pressure of 20 psig. The result of CTE variation as a function of temperature for 2, 3.1, and 5.4 ppm hydrogen containing specimens were shown in Figure 24. The hydrogen was used as a transient alloy addition for Invar. It is apparent that hydrogen addition increases the lattice strain and thus the CTE. This result is the supporting evidence of lattice strain when hydrogen exists in metal.

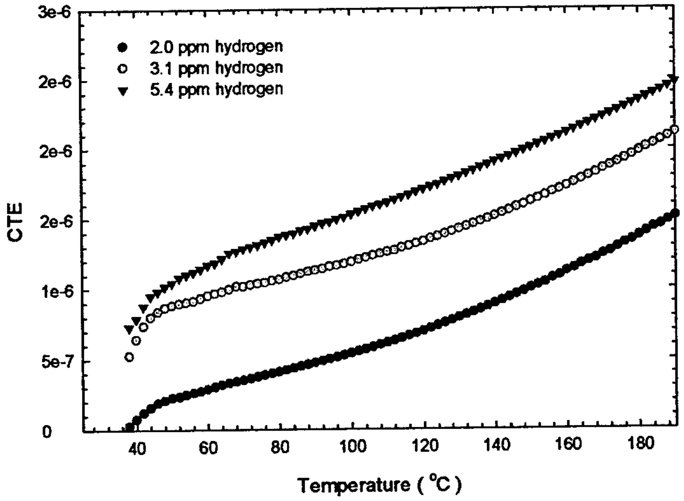

Figure 24. Measured Coefficient of thermal expansion (CTE) as a function of temperature for Invar specimens containing various hydrogen contents.

Figure 25 illustrates the changes in the TEP coefficient with variations in hydrogen content of Invar specimens. The TEP coefficient decreased linearly with increasing hydrogen content. This linear correlation makes the TEP coefficient measurement very convenient and sensitive for assessing diffusible hydrogen content for various alloys. Specifically, alloys with an FCC microstructure can absorb fairly large amounts of hydrogen, which can be measured with the TEP coefficient measurement technique. The TEP coefficient data obtained for Invar shows that small changes in hydrogen contents are also measurable. The results indicate that hydrogen content can be easily determined using TEP coefficient measurement technique with a proper calibration procedure.

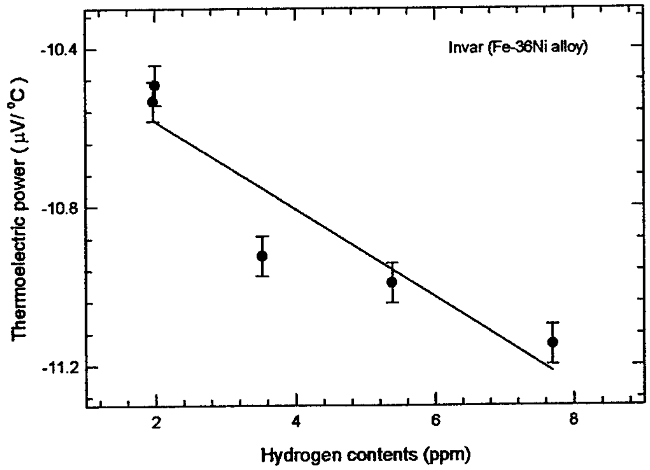

Figure 25. Correlation of TEP coefficients with hydrogen content for Invar (Fe-36Ni) alloys.

Changes in the *d*-band shape is caused by induced strain due to the addition of hydrogen into the lattice. When hydrogen is dissolved in many metals, it occupies interstitial sites in the host lattice causing displacements of the metal atoms from their regular sites. This displacement results in changes in shape of this *d*-band. Hydrogen begins to pull the adjacent two host metal atoms apart resulting in fewer electrons overlapping. When fewer electrons overlap, the energy level of the d-band lowers according to Pauli's exclusion principle, resulting in the narrowing of the *d*-band. The TEP coefficient can detect the changes due to d-band slope change or the effective mass.

2.2.2 Hydrogen Assisted Forming

Enhanced formability in both 2 1/4 Cr-1 Mo steel and TiNb alloy with the use of dissolved hydrogen during the deformation process has been demonstrated.

2.2.2.1. 2 1/4 Cr – 1 Mo steel

The influence of hydrogen on the mechanical properties, especially the yield and flow stress of iron and steels, was investigated quite extensively. However, there are still many controversies on whether hydrogen causes hardening or softening. Hydrogen was long thought to be detrimental to most engineering materials. As was reviewed [14], it appears that the yield and flow stress of iron are increased by hydrogen and the hardening considered to be solution hardening due to hydrogen. Softening was reported only occasionally [15-17]. Kimura, Matsui et al. [18,19] investigated extensively the influence of hydrogen in high purity iron and its alloys in a temperature range of 77 K to near room temperature. Their main conclusion was that the softening and/or hardening effect due to hydrogen is strongly dependent on the impurity of the investigated material and the interaction of hydrogen with impurities. Recently Dong and Thompson [20] confirmed this data by measuring thermal activation parameters. However, an increased understanding e.g. of titanium and titanium alloys [21-25] has demonstrated that hydrogen can become also a powerful tool in improving processing and microstructure/mechanical properties.

Hydrogen induced processing turned out to be very interesting especially for the fabrication of iron and steel. The aim of the following discussion is to present recent results on the improved hot formability of high strength 2 1/4 Cr-1Mo steel in comparison with Armco iron after hydrogenation.

The investigations were performed on commercial Armco iron and 2 1/4 Cr-1Mo steel. Both materials were annealed at 500°C for three hours (in the following identified as as-received) before hydrogen charging and compression testing. EDS analysis showed small amounts of trace elements (e.g. Si, S, Cr, Mn, W) for Armco iron and significant amounts of Si, Mn and Ni for 2 1/4 Cr-1Mo steel. The microstructure was studied by optical microscopy (OM) and transmission electron microscopy (TEM: Philips CM200). For optical microscopy polished specimens were slightly etched with 2% HNO_3 / ethanol. TEM specimens were prepared electrochemical thinning in a solution of 5% perchloric acid and 95% acetic acid at 15°C.

After grinding Armco iron and 2 1/4 Cr-1Mo steel were charged electrolytically with hydrogen in a 2:1 glycerine-phosporic acid electrolyte at 55°C and a current density of $i = 18\ A/m^2$, low enough to avoid charging damage in these materials. Since hydrogen diffusion at RT in the investigated Armco iron and 2 1/4 Cr-1Mo steel is very fast and significant desorption of hydrogen after the hydrogenation had to be avoided for the following mechanical testing, all samples were quenched and stored in an acetone-dry ice bath. Chemical and electrochemical coating of the surface with a supersaturated copper sulfate solution and afterwards with a solution consisting: nickel sulfate, boric acid, ammonium chloride (8:1:1) at a current of about 0.5 A turned out to be very effective to retain hydrogen even during the compression testing. The hydrogen content was measured by a LECO hydrogen determinator. Compession tests were performed with uncharged and hydrogenated samples at strain rates of 5 %/s and 10 %/s at 650°C using a Gleeble 1500. Since this temperature had to be reached at very high heating rates in order to reduce hydrogen loss fluctuations of the temperature of ±10°C as well as of the recorded stress have to be taken into account analyzing the true strain-stress curves.

Effect of Hydrogen on Mechanical Stability

The influence of hydrogen on the compressive mechanical properties, especially the yield and the flow stress of Armco iron and 2 1/4 Cr-1Mo steel was investigated at 650°C for different strain rates of 10 %/s (fig. 26) and 5 %/s (fig. 27).

Comparing the stress-strain curves for uncharged Armco iron and 2 1/4 Cr-1Mo steel at 650°C for strain rates of 10 %/s (fig. 26) and 5 %/s (fig. 27) it can be seen that increasing the strain rate increases the flow stress for both materials.

Figure 28 and 29 reveal only a small, not significant increase of the compressive stress for Armco iron after hydrogenation up to 3.2 wt.ppm hydrogen and compression test at 650°C for strain rates of 10 %/s and 5 %/s, respectively.
In contrast to the results for Armco iron it was observed that hydrogen has a tremendous influence on the yield and the flow stress of the high strength 2 1/4 Cr-1Mo steel. At a strain rate of 10 %/s (fig. 26) and hydrogenation up to 4.5 wt.ppm, 2 1/4 Cr-1Mo steel exhibited a slight decrease in the compressive mechanical properties. However, using a smaller strain rate of 5 %/s after hydrogen charging up to 4.5 wt.ppm hydrogen (fig. 27) lead to a surprising softening effect down to the values of yield and flow stress of Armco iron.

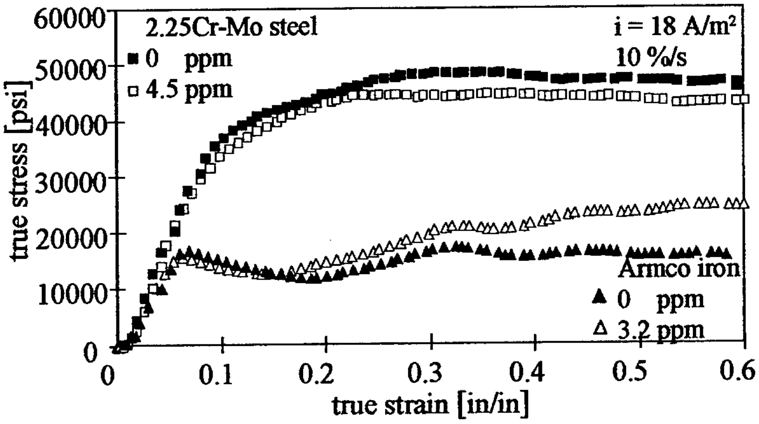

Figure 26. True strain-stress curves of Armco iron and 2 ¼ Cr-1Mo steel at 650°C for a strain rate of 10 %/s **before** hydrogen charging and **after** hydrogen charging.

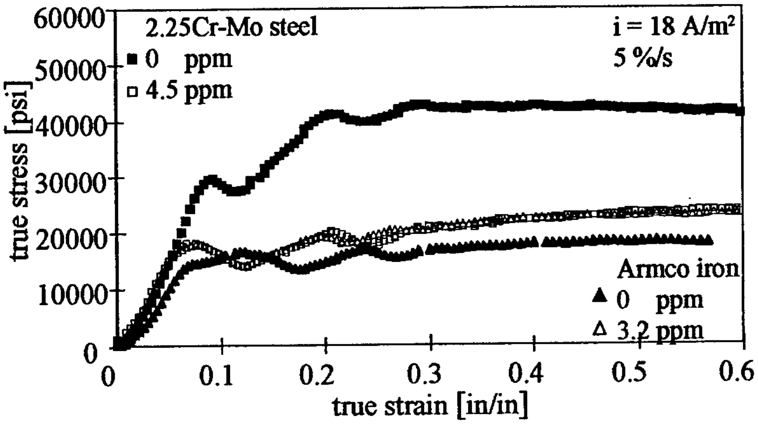

Figure 27. True strain-stress curves of Armco iron and 2 ¼ Cr-1Mo steel at 650°C for a strain rate of 5 %/s before hydrogen charging and after hydrogen charging.

The influence of the hydrogen content on the true strain-stress curve of 2 1/4 Cr-1Mo steel at 650°C was investigated for the high strain rate of 10 %/s (fig. 28). Figure 28 shows that the yield and the flow stress decreased by up to 50 pct. with increasing hydrogen content. At a hydrogen content greater than or equal to 7.8 wt. ppm the similar mechanical properties were observed as for armco iron.

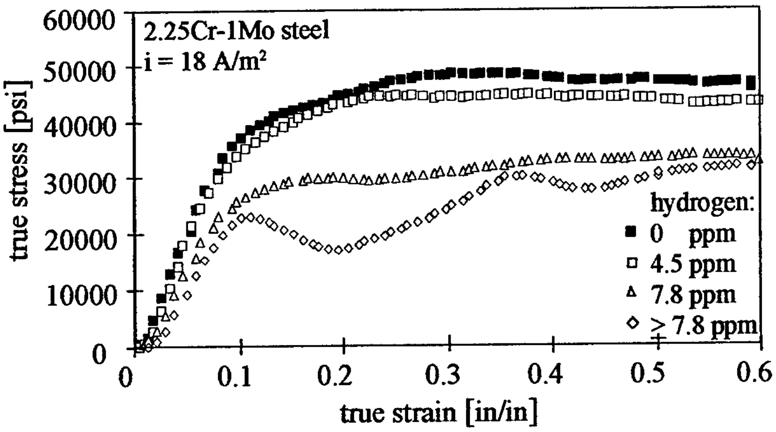

Figure 28. The influence of the hydrogen content on the true strain-stress curve of 2 1/4 Cr-1Mo steel at 650°C for a strain rate of 10 %/s.

Effect of Hydrogen on the Microstructure

Optical microscopy of Armco iron and 2 1/4 Cr-1Mo steel (fig. 29a) in longitudinal direction revealed a ferrite structure for the former and a ferrite-pearlite structure for the latter. Figure 29 (a) and (b) show the microstructure of uncharged and hydrogenated (7.8 wt. ppm hydrogen) 2 1/4 Cr-1Mo steel after compression at a strain rate of 10 %/s. By optical microscopy no significant differences between the uncharged and deformed in comparison to the hydrogenated and deformed material could be observed. TEM investigations of 2 1/4 Cr-1Mo steel (fig. 30) give additional information and allow possible explanations regarding the present mechanism during compression before and after hydrogen charging.

In comparison to the as-received 2 1/4 Cr-1Mo steel (fig. 30a) an increase in the dislocation density as well as the formation of a dislocation network, mostly in the ferrite, was observed after compression at 650°C and a strain rate of 10 %/s (fig. 30b). The observed higher compressive stress of 2 1/4 Cr-1Mo steel might occur due to the formation of dislocations, dislocation networks as well as dislocation pile-ups at the grain boundaries of the ferrite and the very fine lamellar pearlite structure. Hydrogen charging up to 7.8 wt.ppm hydrogen and following compression resulted in a well developed cellular dislocation arrangements which are known from recovery or dynamic recrystallization processes. TEM bright field images (fig. 30c) show clearly the formation of small-angle grain boundaries.

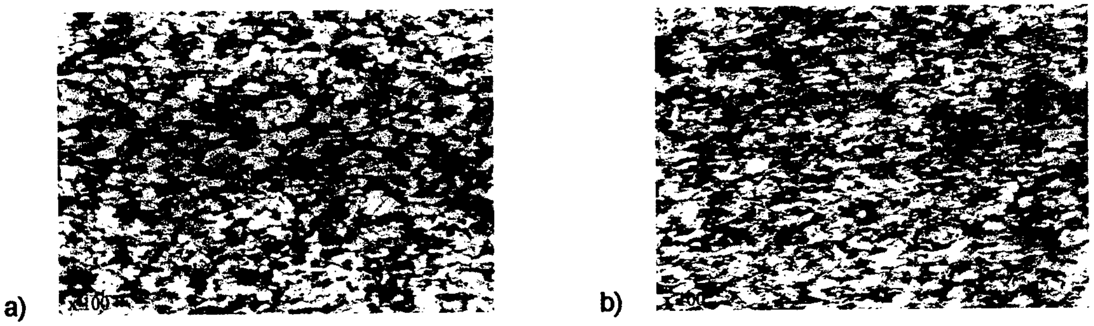

Figure 29. Optical microscopy of 2 1/4 Cr-1Mo in longitudinal direction: (a) uncharged after compression at a strain rate of 10%/s and (b) hydrogen charged (7.8 ppm hydrogen) after compression at a strain rate of 10%/s.

The decreasing strain rate, allows in as-received as well as hydrogenated Armco iron and 2 1/4 Cr-1Mo steel, longer time periods for recovery processes; thus leading to the observed softening effect. The high stacking fault energy, which can be concluded from the ability to form small-angle grain boundaries and the influence of the high temperature on the climbing, cross-slip mechanism of dislocations, and reduced Peierl's potential due to the hydrogen probably increasing the mobility of dislocations in 2 1/4 Cr-1Mo steel. This behavior again should accelerate recovery processes leading to softening with increasing hydrogen content in 2 1/4 Cr-1Mo steel. Such an effect is not observed in Armco iron probably due to an already higher mobility of dislocations without hydrogen. Further studies at lower temperatures are underway in order to verify these assumptions.

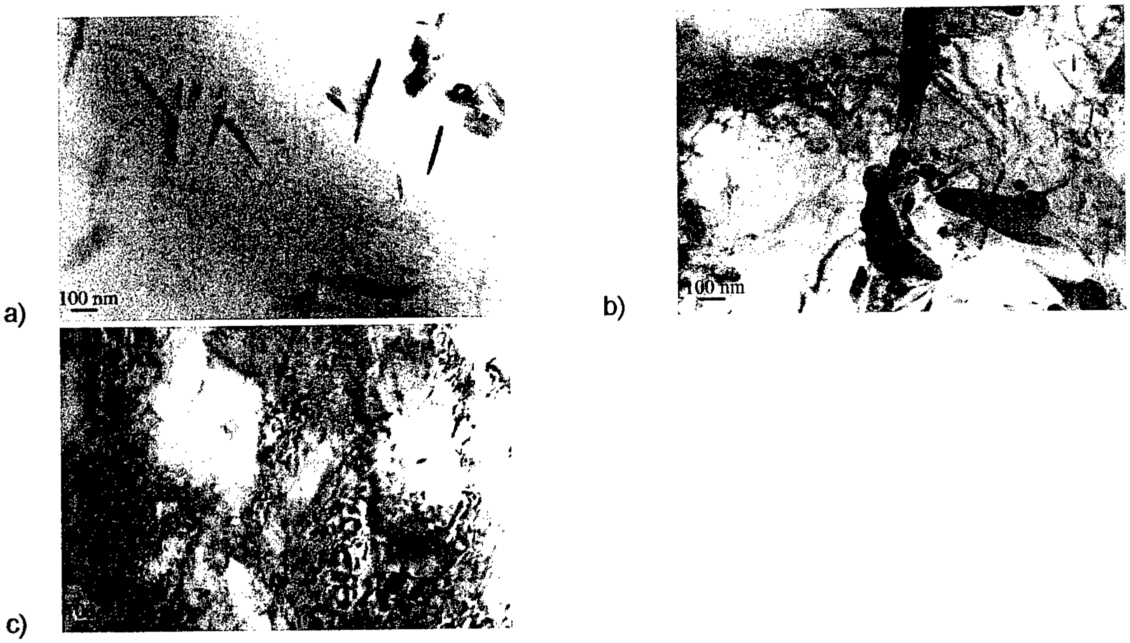

Figure 30. TEM of 2 1/4 Cr-1Mo steel (cross section): (a) as-received, (b) uncharged after compression at a strain rate of 10 %/s and (c) hydrogen charged (7.8 ppm hydrogen) after compression at a strain rate of 10 %/s.

2.2.3 Hydrogen induced plastic deformation in Ti-Nb Alloy

CSM with the collaboration with scientists at Ben Gurian University (Israel) and the University of Dortmund (Germany) performed a similar investigation on hydrogen assisted forming of alloys. The work and results are described in the subsections below.

Alloying of Ti-based alloys with hydrogen has been used to modify the microstructure and improve mechanical properties [26]. Hydrogen charging was performed electrochemically in a 2:1 glycerin-phosphoric acid electrolyte at high fugacities. Hydrogenation of Ti-Nb was found to exhibit a significant effect on the phase stability as well as the microhardness of Ti-Nb alloys. Hydrogenation of Ti-20 wt. pct. Nb led to precipitation of (Ti,Nb)H_x in the metastable α'' matrix. In Ti-Nb alloys with 40 or 45 wt. pct. niobium, hydrogen stabilized the bcc β-phase, but destabilized the hcp α-phase. With increasing hydrogen content an expansion of the lattice constant of the β-phase occurred, followed by the formation of (Ti,Nb)H_x. The influence of hydrogen on the microhardness of Ti-40 wt.pct.Nb and Ti-45 wt.pct.Nb shows only a minor effect, whereas Ti-20 wt.pct.Nb exhibits significant softening in response to hydrogen charging up to 3000 ppm. TDS showed that deuterium desorption strongly depends on the niobium content and the deformation treatment prior or after charging.

The observed results should provide further insight on the mutual effects and the resulting micromechanism of hydrogenation and deformation in Ti-Nb alloys. The studies of sintered Ti-20 wt.pct. Nb and Ti-40 wt.pct. Nb, as well as of commercial Ti-45 wt.pct.Nb, showed a strong influence of hydrogen at high fugacities on phase stability and microhardness as well as on the thermal desorption of the hydrogenated Ti-Nb alloys which were deformed before or after deuterium charging.

The microhardness of sintered Ti-20 wt.pct.Nb decreased significantly during hydrogenation at high fugacities. The observed softening might occur due to a change in the α''/β ratio during the precipitation of (Ti,Nb)H_x as mentioned above.

Microstructural investigations of Ti-40 wt.pct. Nb and Ti-45 wt.pct. Nb alloys reveal the bcc β-phase as well as the diffuse ω-phase. Cathodic hydrogen charging leads to stabilization of the bcc phase, but to destabilization of the hcp ω-phase. An expansion of the lattice constant of the ϖ-phase and the formation of (Ti,Nb)H_x could be observed in Ti-45 wt.pct. Nb.

The microhardness showed only a minor change after hydrogenation for Ti-40 wt.pct.Nb and for Ti-45 wt.pct. Nb alloys. It is assumed that the minor decrease of the microhardness in Ti-45 wt.pct. Nb is due to the destabilization of the ω-phase during hydrogen charging and the following increase due to the precipitation of (Ti,Nb)H_x.

Thermal desorption analysis showed that desorption of deuterium in Ti-Nb (20-45 wt.pct. Nb) is influenced by the niobium content, most likely by the phases present. The desorption temperature increases with the niobium content. Deformation prior to deuterium charging led to an increased desorption temperature. One explanation for this influence could be that trapping sites formed during the deformation have a stronger affinity for deuterium and/or deuterium segregates at dislocation cores.

Deuterium charging followed by deformation of Ti-45 wt.pct. Nb, however, leads to a reduced desorption temperature, probably due to an increased amount of screw dislocations generated during the deformation of the hydrogenated ω-phase [27].

2.3 Hydrogen Management in Structural Alloy Welds

Hydrogen-assisted cracking is the most common cracking problem encountered during the fabrication of welded steel structures [28]. With the advances in high strength low alloy (HSLA) steel processing, cracking has moved from the HAZ to the weld metal. The susceptibility to hydrogen embrittlement has been primarily related to the steel composition, microstructure and temperature [29]. Current preventive measures such as pre- and/or post-weld heat treatment, proper electrode selection and handling, and edge preparation have been used to minimize the hydrogen concentration and stress level [25]. Through these practices, HSLA steel welds can maintain acceptable levels of hydrogen content as low as one to two milliliters of hydrogen per 100 grams of weld deposit. However, these practices require much effort, time and expense.

For better understanding of HAC for steel weldments, two classifications of hydrogen must be considered. Diffusible hydrogen is the mobile hydrogen that is available for diffusion to the tri-axial stress sites and is considered to potentially harmful for HAC. The residual hydrogen is the hydrogen that is trapped at specific sites in the microstructure, preventing its transport. The prevention or control of diffusible hydrogen in the weld metal may reduce the susceptibility to hydrogen cracking.

2.3.1 Hydrogen Trapping as a Method to Manage Weld Metal Hydrogen Damage

It has been reported [30-32] that diffusible hydrogen can be suppressed by introducing selected rare earth metal and transition metal additions, as powder ferroadditions, to the weld metal to serve as hydrogen traps. These traps, in the form of oxides or carbonitrides, have high binding energies with hydrogen. Fundamental investigation has been done by Maroef [33] by using neodymium and yttrium as hydrogen trapping elements in iron and low carbon steel. The yttrium resulted in the most effective trap, due to its higher weld metal recovery than that of neodymium, thus reducing in the diffusible hydrogen content by forty percent of that of a steel weld made with no yttrium addition.

Baune [34] investigated the use of cerium fluoride and cerium oxide in basic flux cored welding electrodes and showed that cerium fluoride had a slightly better effect in reducing the diffusible hydrogen content than cerium oxide. The cerium fluoride had the advantage of the fluoride reducing the activity of the hydrogen in the weld arc plasma which may contributed to the decrease in diffusible hydrogen as well as the high reactivity of cerium. However, arc characteristic behavior, i.e. arc stability, by the addition of these cerium compounds were not discussed. Pokhodnya [31] showed that the diffusible hydrogen content in the weld metal could be reduced by microalloying it with rare-earth hydride-forming elements. The redistribution of the diffusible hydrogen has decreased with increasing rare-earth content, corresponding to an increase in residual hydrogen content. The oxy-sulfide form of the rare-earth compound was found to be the trapping inclusion in the steel weld metal alloyed with manganese, nickel, and molybdenum.

Eberhart [32] postulated an orbital model to rationalize the effectiveness of traps in bcc iron. Throughout this model, it is argued that the binding energy of hydrogen to traps is largely determined through the Fermi energy orbital topology at the trap-bcc iron interface. Estimates of trapping efficiency for several inclusions in steel were conducted using this model. As a result, Ce_2O_3 was predicted to be the most effective trap followed by TiC, Y_2O_3, NbC, and finally Mo_2C. Titanium carbide has a binding energy of approximately 100 kJ per mole.

The investigation first experimentally determined if hydrogen traps are effective in HSLA steel welding and evaluate the performance of each selected rare earth metal and transition metal hydrogen traps in HSLA weldments in order to reduce the susceptibility to HAC. The diffusible hydrogen measurement and the verification of these traps will be determined by gas chromatography, thermal desorption analyses, and metallographic techniques and XRD analysis, respectively.

The first investigation was followed by studying effects of welding parameters on diffusible hydrogen levels in the advancement of hydrogen management. The influence of the welding parameters(including amperage, voltage, travel speed, and transfer mode, as well as the interrelationship) on the utility of hydrogen traps in managing diffusible hydrogen content is studied.

2.3.2 Irreversible Hydrogen Trapping in High Strength Steel Weldments

The effectiveness of irreversible hydrogen traps in HSLA steel weld metal investigated to observe if the diffusible hydrogen content of a HSLA steel weld deposit can be reduced. The addition of neodymium in the HSLA steel metal cored wire shows a slight increase in the diffusible hydrogen content compared to that of the HSLA steel base reference. Because a neodymium rich intermetallic phase with iron does not exist, the difficulty of introducing neodymium as a ferro-neodymium powder is not practical and other factors such as the transfer behavior and thermochemical reactions may play an important role for such a reactive element.

2.3.2.1 Metal Core Wires

Four types of irreversible traps, titanium, vanadium, neodymium and yttrium, were used in the form of ferropowders that were fabricated at CSM. These powders were made by forming the brittle intermetallic phase with iron and then crushed and sized by immersion in liquid nitrogen. Three content levels for each trap type were used to study the effect of the amount of traps available for hydrogen trapping. The mild steel sheath was made with three yttrium additions of 500, 1000, and 2000 ppm. The HSLA steel sheath was made with neodymium (500, 1000, and 2000 ppm), titanium (200, 300, and 400 ppm), and vanadium (200, 300, and 400 ppm). These metal cored wires were drawn to 0.0625 in. (1.6 mm) in diameter electrodes.

2.3.2.2 Diffusible Hydrogen Measurement

Diffusible hydrogen measurements were carried out following the ANSI/AWS A4.3-93 [34]. The weld specimens for this procedure were cut from HSLA 100 steel plate and were either mechanically milled or grounded to the dimensions of 12 mm x 25 mm x 40 mm and measured to maintain tolerances specified in the standard method. High strength low alloy (HSLA) steel was supplied by the U.S. Steel Company and was used for all welding experiments as the base plate in both phases of this research.

Once the weld specimens had been prepared, the specimens were hydrogen degassed at 600°C for at least six hours in a vacuum furnace. Any subsequent oxide formation was immediately dry ground. The specimens were weighed, recorded, and welded. After welding, the samples were ice quenched within five seconds of completion of weld for twenty seconds. The weld samples were then stored in a dry ice and acetone mixture (-72 °C). When all welds were made, the samples were dry sand blasted and the samples for diffusible hydrogen measurement were returned to the dry ice/acetone bath.

The gas chromatograph method proposed by Quintana et al. was used for the measurement of diffusible hydrogen. The gas chromatograph method allows for lower levels of hydrogen detection to one part per million content due to the sensitivity of the thermal conductivity detector used in gas chromatography. The sampling of the diffusible hydrogen gas from the canister required using a one milli-liter syringe to inject the gas sample into the gas chromatograph for analysis. The ambient temperature and barometric pressure were recorded for each measurement. Initially, a standard gas mixture of hydrogen and helium was tested to verify reliable measurements before the samples were tested. At least three injections were made for each sample in which results were in a good agreement and the pressure of each canister was checked for any leaking.

The thermal desorption analysis was used to verify the high temperature trapping of hydrogen in the HSLA steel weldments. A four degrees per minute heating rate was used and the measurement was carried out to 1000 °C.

2.3.2.3 Characterization of Hydrogen Traps

The bromine method was used to extract non-metallic inclusion in the weldments. The bromine method is useful in recovering non-metallic inclusions in steel; the iron matrix is dissolved in the bromine solution, leaving behind the non-metallic inclusions. These inclusions were collected by filtering and then washed before analysis. A Phillips XRD machine was used and the resulting XRD spectral was used to identify the inclusions.

Induced Couple Plasma (ICP) analysis was used to obtain the chemical composition of the weldments and metal core electrodes. ICP analysis samples are prepared by dissolving a small amount, about 0.1 grams, in a concentrated nitric acid solution. The solution is vaporized by plasma and detected by spectroscopy. The ICP method is useful when the material is completely dissolved, which may not be the case for certain oxides.

2.3.2.4 Welding Parameters

Iron fill metal-cored steel wire (plain carbon steel sheath) was made to serve as a base line wire. Iron fill metal-cored wires were made, containing four levels of ferro-yttrium (Fe_2Y) content. The yttrium contents in the iron fill metal cored wire are approximately 0, 350, 3000, and 6000 ppm. Three levels were chosen to study the effect of welding parameters and trap content and the wire with no yttrium served as a baseline. Iron filled metal-core wires had a powder fill of about fifteen weight percent and AISI-SAE 1005 plain carbon steel sheath. Details of the tubular wire bench forming operation and flux/powder flow characterization are discussed in another reference. Powder flow characteristics, such as flow rate and composition, were performed on ferro-yttrium powders with a size range between 200 to 600 microns. Mass flow rate and sampling at thirty second intervals for composition distribution were performed and resulted in a uniform flow rate, as well as a uniform composition.

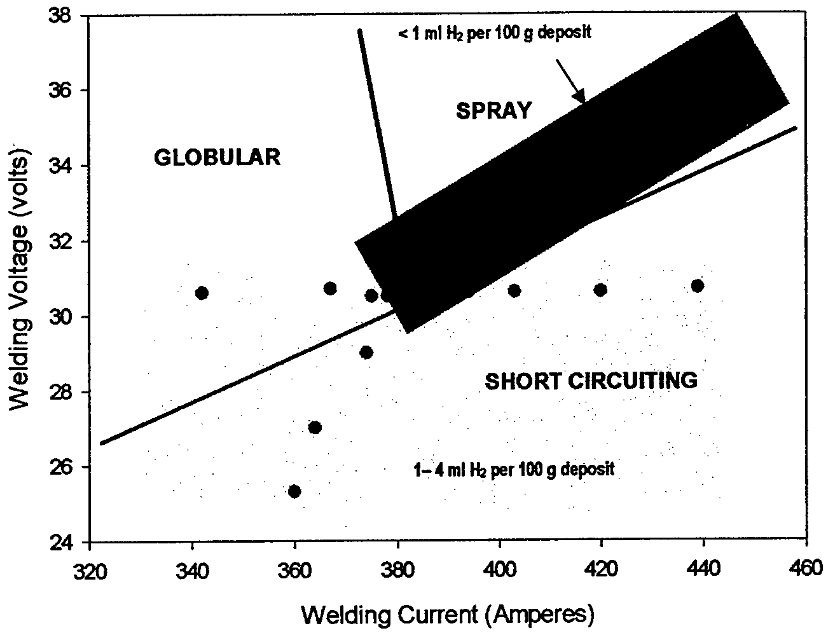

Figure 32. Metal transfer mode – weld metal diffusible hydrogen content plot on a GMA welded HSLA steel with HSLA steel metal cored steel wire containing 1600 ppm yttrium.

A metal-cored wire with a HSLA steel composition was also fabricated with about 1600 ppm of yttrium and its chemical composition. The same standard procedure was used in phase one for the measurement of diffusible hydrogen. These wires were used to study the weld parameters on the diffusible hydrogen content for phase two of this research. The test matrix has been established to vary the heat input by varying the voltage while the current (wire feed speed) and travel speed remain constant. Voltages were chosen for much of the complete range where welding was possible. Similarly, the current was varied and the voltage and travel speed was held constant. The effect of travel speed was varied while voltage and current were held at a constant value. The effects of oxygen content, introduced through the shielding gas, was examined by using four levels of oxygen (0, 1, 2 and 4 percent oxygen-balance argon). The metal transfer modes and resulting diffusible hydrogen contents with variation of welding current and voltage is shown in Figure 32.

2.3.3. New Approach to measure diffusible hydrogen contents in HSLA steel weld metal

To correlate TEP coefficient values with various hydrogen content levels in welds, measurements of actual diffusible hydrogen of welded HSLA steel with increasing hydrogen concentration in shielding gas were conducted according to the procedure detailed in ANSI/AWS A4.3-93, which is shown in Appendix A. The hydrogen content of the argon shielding gas was increased to a level of 6 percent by volume. The welding parameters were kept same as described in experimental procedures.

The diffusible hydrogen content of the welds as a function of volume pct. hydrogen in the shielding gas is shown in Figure 33. The result indicates that no detectable diffusible hydrogen was detected for 0 vol. pct. hydrogen in shielding gas. As volume pct. of hydrogen increase, the amount of diffusible hydrogen increases in parabolic function. Since the welding is conducted under controlled laboratory conditions, it appears that Sievert's law is valid. In Figure 34, the volume percent of hydrogen has been converted to partial pressures assuming ideal gas behavior and an overall pressure of one atmosphere around the weld.

With results of correlation between diffusible hydrogen content and hydrogen vol. pct. in shielding gas, TEP coefficient measurements were conducted for welded HSLA steels with various hydrogen vol. pct. in argon shielding gas. After the welding, welded specimens were stored in liquid nitrogen until measurement began. Therefore, the initial sample temperature of measurement was around -150 °C and rose to room temperature.

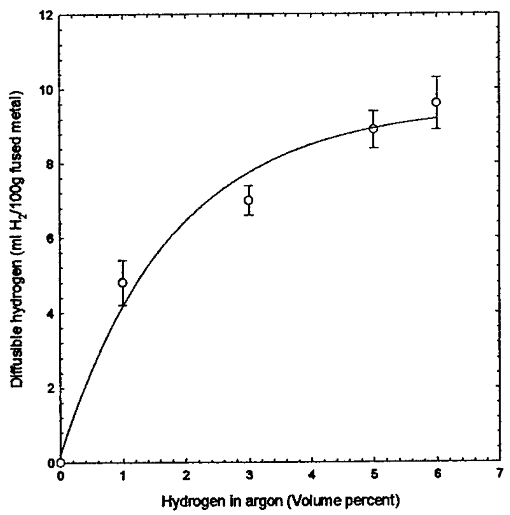

Figure 33 Measured diffusible hydrogen content of weld metal as a function of hydrogen volume percent.

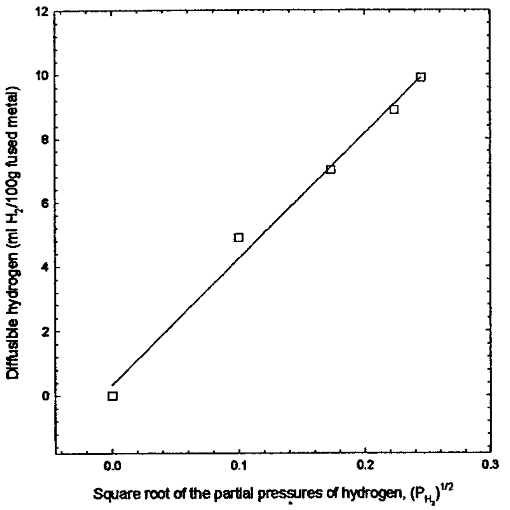

Figure 34 Measured hydrogen content of weld metal as a function of the square root of the partial pressure of H_2 above weld pool.

TEP coefficient measurements of welded HSLA steel using 0 vol. pct. hydrogen and 6 vol. pct. hydrogen-argon mixture are shown in Figure 35. One of the striking result is the large difference in TEP coefficient between 0 and 6 vol. pct. hydrogen at low temperature (about –140 °C) between two welded specimens. As specimen temperature increased to room temperature, TEP coefficient curves of two specimens approach almost the same value. The TEP coefficient value is not exactly same, and the reason for that is discussed in a different chapter. The result indicates that TEP coefficient value is amplified when specimen temperature is lower than room temperature, and the differences increase as specimen temperature decrease. This amplification effect, which was not possible at room temperature, makes the use of TEP coefficient for hydrogen sensor very valuable. One other advantage of this low temperature measurement is that welded specimen storage in low temperature media, such as liquid nitrogen or mixture of dry ice and acetone, is that it is consistent with the standard procedures for diffusible hydrogen measurement according to ANSI/AWS A4.3-93.

Other hydrogen contents, 1, 3, and 5 vol. pct. in shielding gas, were welded, and TEP coefficient measurements were conducted to correlate with diffusible hydrogen content. The results of TEP coefficient measurements of these welded specimens are shown in Figure 36. As diffusible hydrogen content increases, each TEP coefficient curve moves to a lower level, systematically. These results suggest that the plot of TEP coefficient as a function of either time or specimen temperature can be used to curve fit a standard plot to determine the resulting diffusible hydrogen content for steel weld metal. For example, field practitioners may take the TEP coefficient measurement device and measure the TEP coefficient value of actual welds in low temperature by recording a specimen temperature. The measured TEP coefficient value can be compared with a plot of the TEP coefficient as a function of time or specimen temperature, and basically indicates the hydrogen content in the welds. This approach using TEP coefficient measurement at low temperature makes diffusible hydrogen content measurement much easier and faster. The time required for measurement is about thirty times faster as compared to conventional standard diffusible hydrogen measurement methods.

Figure 37 presents the measured TEP coefficient as a function of specimen temperature. Each curve becomes more linear line when TEP coefficient was plotted as a function of sample temperature. These results indicate that each TEP coefficient curve represents amount of diffusible hydrogen in HSLA steel welds. Therefore, by recording both the TEP coefficient value and specimen temperature for diffusible hydrogen measurement practice, instantaneous amounts of diffusible hydrogen for weld metal can be obtained.

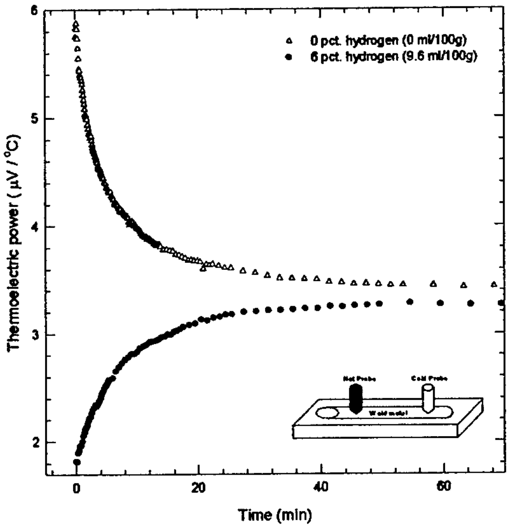

Figure 35 Measured TEP coefficient of welded HSLA steel with UHP argon gas (0 vol. pct. hydrogen) and 6 vol. pct. hydrogen-argon mixture in shielding gas for 79 minutes. Welding condition: 120 Amps, 1 mm/s travel speed, ice water quenching, and liquid nitrogen storage.

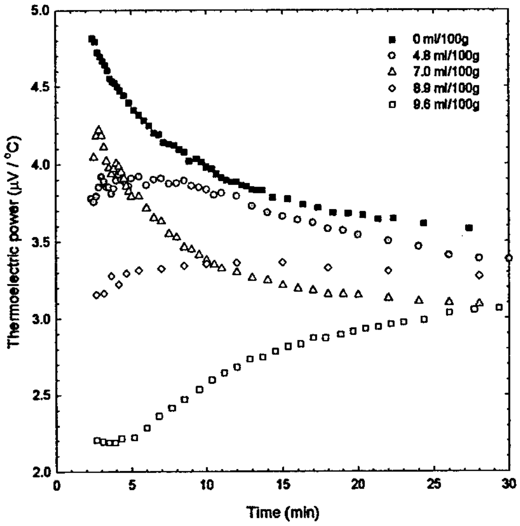

Figure 36 Measured TEP coefficient of welded HSLA steel with five different hydrogen content levels (0, 1, 3, 5, and 6 vol. pct.) in shielding gas for thirty minutes. Actual diffusible hydrogen content is shown in legend. Welding condition: 120 Amps, 1 mm/s travel speed, ice water quenching, and liquid nitrogen storage.

The TEP coefficients of certain sample temperature, -60 and -40 °C, were taken and plotted as a function of diffusible hydrogen content. The results are shown in Figure 38 (a) and (b). The results indicate that TEP coefficient is relatively linear with amount of diffusible hydrogen in welded HSLA for both sample temperature of -60 and -40 °C. However, reproducibility of the TEP coefficient measurements for welded HSLA steel with 3 and 5 vol. pct. hydrogen additions in shielding gas was not poor. It appears that poor reproducibility of measurements mainly caused by experimental difficulties due to low temperature measurement. As soon as the specimen is placed in the measurement set-up, the temperature controllers are trying to maintain the differential temperature as 10 °C, and it takes about 5-10 minutes to achieve stable differential temperature of 10 °C. Also, pressure of probes on specimens found to be very critical at low temperature. Thus, measurement technique as well as TEP ánalysis set-up needs to be developed for improved reproducibility of measurement.

In addition, analytical hydrogen content sensor using TEP coefficient needs to be accurate and calibrated to hydrogen content as low as 0.1 ml per 100 g of metal (0.089 ppm hydrogen). This step is very challenging, but can be improved with the development of measurement set up and accurate calibration procedure. The other design requirement is that the analytical apparatus must be easy to operate and understood by technicians in the welding workplace, and the data must be easily acquired and stored electronically in a computer. The measurements must be able to be made directly on welds in the welded structure, as well as measured on test coupons. The equipment must be sufficiently durable and lightweight to be conveniently used in the welding workplace.

According to experimental results, the sensor using TEP allows measurement of diffusible hydrogen content directly from a welded structure, eliminating the need for duplicate specimen coupons. The sensor generates the necessary analytical signal in less than fifteen minutes after cooling from liquid nitrogen, and can be calibrated to yield results in ml H_2/100 g weld metal. A design incorporating an array of sensors or a motorized sensor could be used to generate diffusible hydrogen distributions with a high resolution.

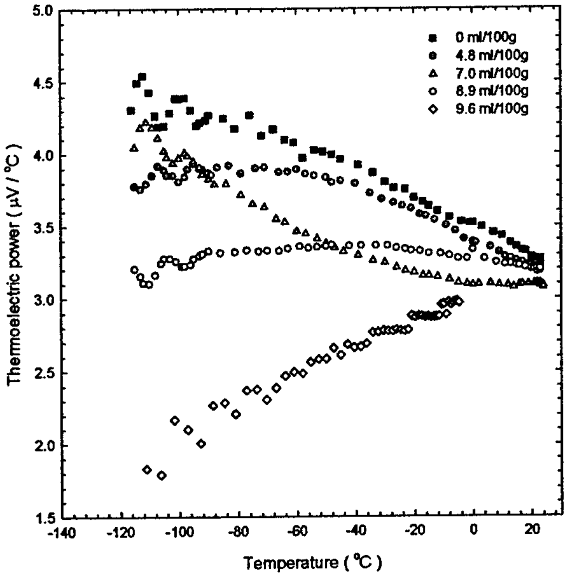

Figure 37 Measured TEP coefficient as function of specimen temperature for all five welded HSLA steel specimens.

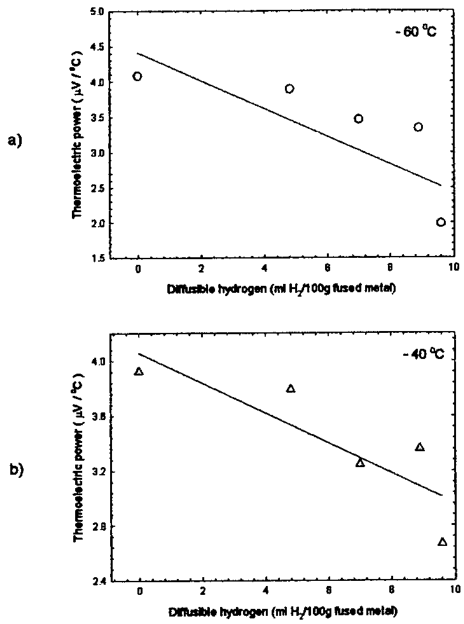

Figure 38 Measured TEP coefficient as a function of hydrogen content vol. pct. in shielding gas at specimen temperature of a) -60 and b) -40 °C.

2.4. Thermoelectric Power Sensor to Assess Nitrogen Content

The results of total nitrogen content for plasma welds of stainless steel Alloy 1.4565 are shown in Table 2 for each different analytical technique used for the determination of total nitrogen content. A comparison of the results of total nitrogen content for each method indicates that there is no standardization for total nitrogen content determination.

Table 2 shows the results of measuring both the total nitrogen content and the interstitial nitrogen content of stainless steel Alloy 1.4565 utilizing the Leco nitrogen determinator and Beeghly's ester-halogen process. These results indicate that approximately two percent nitrides are present in the base metal Alloy 1.4565, with approximately 15 - 19 percent of the nitrogen in the weld metal being formed nitrides. Table 3 represents the thermoelectric power coefficient indicating the interstitial nitrogen content present in weld pass or remelt weld pass in the autogeneous welding of stainless steel Alloy 1.4565.

Table 2: Total nitrogen measurements from various analytical techniques for stainless steel Alloy 1.4565.

	Total Nitrogen Content (wt %)		
# of Weld Passes	Leco Nitrogen Determinator	Spark Emission	Micro-Kjeldahl
1	0.551	0.403	0.5
2	0.5072	0.376	0.5
3	0.6043	0.391	0.49

Table 3: Comparison of total nitrogen content, nitride content, and interstitial content for stainless steel Alloy 1.4565.

# of Weld Passes	Weld Metal Total Nitrogen (wt%)	Weld Metal Nitride Content (wt%)	Weld Metal Interstitial Nitrogen (wt%)	% Interstitial Nitrogen in Weld Metal	% Nitrides in Weld Metal
1	0.551	0.0822	0.4688	85.08	14.92
2	0.5072	0.09541	0.4118	81.20	18.81
3	0.6043	0.1178	0.4865	80.51	19.49

Table 4: Interstitial nitrogen content from Beeghly process and thermoelectric power coefficient for stainless steel Alloy 1.4565.

	Interstitial Nitrogen Content	
# of Weld Passes	Leco & Beeghly Process (wt%)	Thermoelectric Power (µV/C)
1	0.4688 ± .0040	5.009
2	0.4118 ± .0040	5.124
3	0.4865 ± .0060	4.976

Figure 39 is the thermoelectric power coefficient as a function of total nitrogen content for plasma welded stainless steel Alloy 1.4565. Figure 40 is the results for stainless steel Alloy 1.4565 GTA welds showing the same trend (opposite concavity) of non-linear behavior. A linear relationship does not exist between the thermoelectric power coefficient and total nitrogen content for either plasma or GTA welded stainless steel Alloy 1.4565 welds. However, a linear relationship does exist for the Seebeck coefficient as a function of interstitial nitrogen content for all welds, which is shown in Figure 40 for plasma-welded stainless steel Alloy 1.4565. As the interstitial nitrogen content is decreased due to the formation of nitrides, the Seebeck coefficient consequently increases.

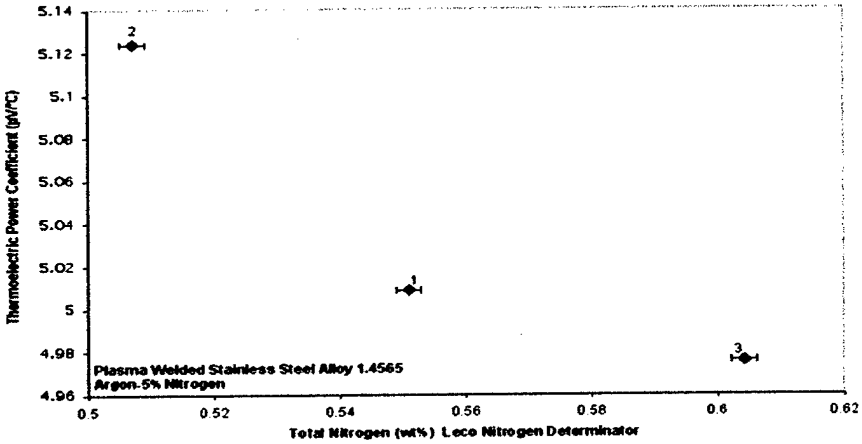

Figure 39 Thermoelectric power as a function of total nitrogen content for plasma welded stainless steel Alloy 1.4565 with argon-5% nitrogen shielding gas . 1,2, and 3 indicate the number of weld passes.

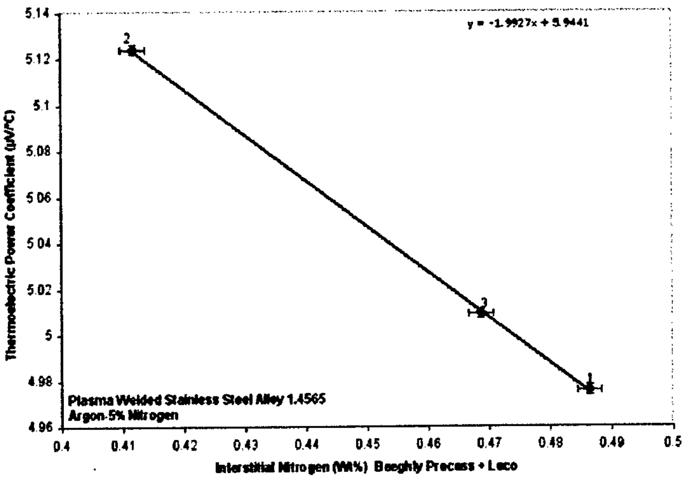

Figure 40: Thermoelectric power as a function of total nitrogen content for plasma welded stainless steel Alloy 1.4565 with argon-5% nitrogen shielding gas . 1,2, and 3 indicate the number of weld passes.

An SEM image is shown in Figure 41 (a) of the austenitic plasma weld metal (three weld passes) indicating a dendritic cored solidification structure with an interdendritic region full of nitrides. Figure 41 (a) is then zoomed in to 1500x (Figure 41 (b)) and a line scan is run to determine the phases that make up the dendritic solidification. The line scan is performed along the arrow shown in Figure 41 (b). The line scan results shown in Figure 6.10 verifies the cored primary austenite solidification.

(a)

(b)

Figure 41: (a) SEM image of stainless steel Alloy 1.4565 (triple plasma weld passes) at 800 X and (b) at 1500X. Note that yellow arrow corresponds to EDX scan line of the solute compositional profile shown in Figure 40.

To determine the composition of the interdendritic region, X-ray diffraction was used and the results are shown in Figure 6.13. The X-ray diffraction measurement on the residue from the nitride analysis indicates that there are dispersed formed nitrides in stainless steel Alloy 1.4565.

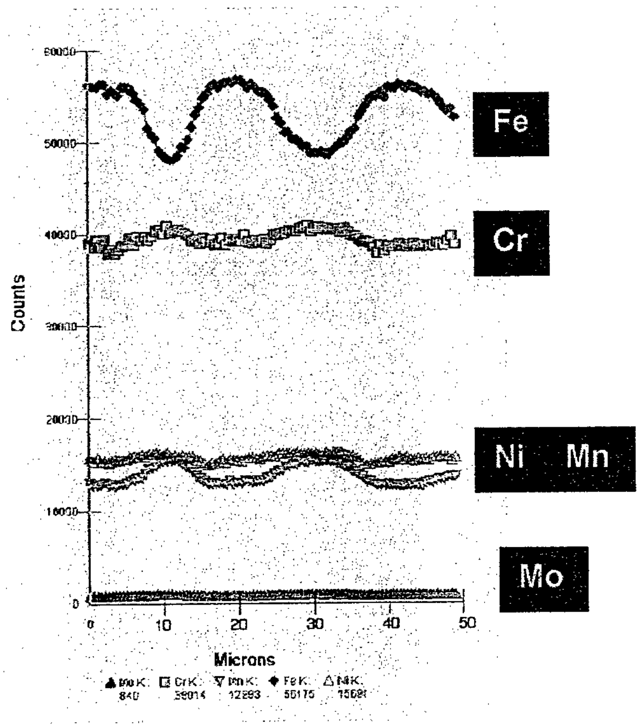

Figure 42: Scanning Electron Microscope energy dispersive x-ray analysis of plasma welded stainless steel Alloy 1.4565.

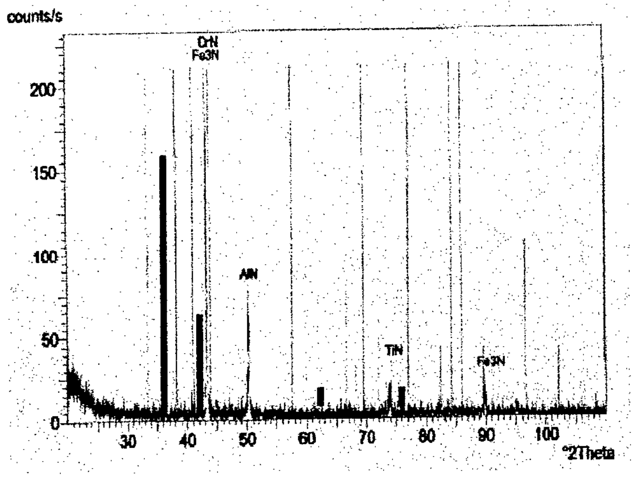

Figure 43. X-ray diffraction scan of plasma-welded (triple pass) stainless steel Alloy 1.4565.

The largest peak is hexagonal close-packed Fe_3N, which overlaps a hexagonal close-packed CrN peak. These results show that nitrides do in fact form during welding of high austenitic stainless steel Alloy 1.4565, thus increasing the importance of analysis and characterization of nitrogen as an alloying addition. X-ray diffraction also verifies that the interdendritic chromium has reacted with nitrogen resulting in interdendritic chromium nitride formation. Adjacent to the chromium nitride, chromium is depleted, which could potentially lead to chromium sensitization. Chromium sensitization adjacent to the formed nitrides may also promote pit initiation adjacent to the nitride, particularly in the interdendritic regions where the nitrogen content is high, thus promoting the formation of nitrides as shown in the micrographs in Figure 40.

A thermodynamic expression of equilibrium was applied to demonstrate the relationship between the Seebeck coefficient and nitrogen phases during homogenization. Making a correlation between all of the results presented was important for a thorough analysis. The results of the total nitrogen contents were inconsistent between different analytical techniques for stainless steel Alloy 1.4565 samples as shown in Table 2. Plotting thermoelectric power as a function of total nitrogen as in Figure 39. It became obvious that it was important to determine what was actually being measured in terms of nitrogen content. The solubility diagram of stainless steel Alloy 1.4565 showed that the nitrogen solubility is exceeded at 1500 °C, leading to the formation of nitrides during welding. Then applying Beeghly's ester/halogen method, a quantitative nitride content was found proving that nitrides had formed during the solidification process. A second verification of the existence and type of nitrides formed came from x-ray diffraction. From the scanning electron microscope images it is possible to see that nitrides formed in the interdendritic region. Knowing that the equilibrium partition coefficient is less than one for nitrogen and most other alloying elements in iron resulting in segregation, which is verified in the SEM line scan across the weld (dendritic and interdendritic) shown.

The modification of the Ellingham-Richardson diagram accounting for high nitrogen content and alloying elements present in stainless steel Alloy 1.4565 showed the thermodynamic order of formation of nitrides with chromium being the first to form. The Seebeck coefficient as a function of total nitrogen content from Figure 40 and the interstitial nitrogen content from Figure 41 for plasma welded stainless steel Alloy 1.4565 experimentally agrees with the thermodynamic models are discussed (36). Speculating from the thermodynamic models, the Seebeck coefficient is extremely sensitive to microstructure. The interstitial nitrogen is constant in the dendritic region, so the only changes occurring during welding are the changes in the interstitial nitrogen in the interdendritic region. The Seebeck coefficient is monitoring the change of the interstitial nitrogen in the interdendritic region.

2.5 References

1. C.D. Gelatt, *Theory of Alloy Phase Formation*, TMS/AIM, Warrendale, Pa, pp.451 (1980).
2. W. Pepperhoff, M. Acet, "Constitution and Magnetism of Iron and Its Alloys", Springer-Verlag Berlin, Germany, 2001.
3. AWS, "Carbon and Low Alloy Steels," Welding Handbook, vol. 4, 7th ed., edited by W.H. Kearns, AWS, Miami, FL, 1982.
4. R.C. Shutt and D.A. Fink, "New Considerations for the Measurement and Understanding of Diffusible Hydrogen in Weld Metal," Weld. J., vol. 64, no. 1, Jan., 1985, pp. 19-28.
5. N. Bailey, F.R. Coe, T.G. Gooch, P.H.M. Hard, N. Jenkins and R.J. Pargeter, "Welding Steels without Hydrogen Cracking," Abington Publishing, Cambridge, 1989.

6. N. Yorioka and H. Suzuki, "Hydrogen Assisted Cracking in C-Mn and Low Alloy Steel Weldments", Intl. Matls. Review, vol. 35, no. 4, 1990, p.217.
7. I.S. Maroef and D.L. Olson, "Fundamental Aspects of Hydrogen Trapping in Steel Weld Metal", in Joining of Advanced and Specialty Materials II, pp. 227-235, ASM Conf., Cincinnati, OH, November 1-4, 1999, ASM, Materials Park, OH (2000).
8. D. Zander I. S. Maroef, D. L. Olson and D. Eliezer, "Positive Effect of Hydrogen on the Plasticity of 2 1/4 Cr- 1Mo Steel". J. Alloys and Compounds, Vol 365-367, p 809-817 (2003)
9. W. Pepperhoff, M. Acet, "Constitution and Magnetism of Iron and Its Alloys", Springer-Verlag Berlin, Germany, 2001.
10. Rozenak, P and Eliezer, D., "Phase Changes Related to Hydrogen-Induced Cracking in Austenitic Stainless Steel", Acta Metall., Vol. 35, No. 9, pp. 2329-2340, Sept. 1987.
11. Uwakweh, ONC; Genin, J-MR; Silvain, J-F, " Hydrogen Cathodic Charging of High Carbon Binary Steel and Martensitic Induced Transformation," Scripta Metallurgica et Materialia, vol. 24, No. 6, June 1990, pp. 1075-1079.
12. K.H.J. Buschow and R.C. Sherwood, *J. Appl. Phys.* **49**, 1480-1485 (1978).
13. Wang and S. Suda, *J. Alloys Compounds* **191**, 5-7 (1993).
14. E. Lunarska, Hydrogen degradation of ferrous alloys, eds.: R.A. Oriani, J.P. Hirth, M. Smialowski, Park Ridge, NJ, Noyes Publication (1985), pp. 321.
15. C.D. Beachem, Met. Trans. 3 (1972), 437.
16. I.M. Bernstein, Scr. Met. 8 (1974), 343.
17. H. Matsui, S. Moriya, H. Kimura, Proc. 4th Int. Conf. Strength of Metals and Alloys, Nancy, France (1976), 291.
18. H. Kimura, H. Matsui, A. Kimura, T. Kimura, K. Oguri, in: Proc. 3rd Int. Conf. on Effects of Hydrogen on Behavior of Materials 1980, eds.: I.M. Bernstein, A.W. Thompson, The Metallurgical Society of AIME (1981), pp. 191,
19. H. Matsui, S. Moriya, H. Kimura, Mat. Sci. Eng. 40 (1979), 207,
20. H. Dong, A.W. Thompson, Mat. Sci. Eng. A188 (1994), 43,
21. U. Zwicker et al.: U.S. Patent No. 2,892,742, June 1959,
22. W.R. Kerr, P.R. Smith, M.E. Rosenblum, F.J. Gurney, Y.R. Mahajan, L.R. Bidwell, in: H. Kimura, O. Izumi (Eds.), Proc. 4th Int. Conf. Titanium, Kyoto, Japan, AIME, Warrendale, PA, 1980, 2477,
23. F.H. Froes, D. Eliezer, H.G. Nelson, The Minerals, Metals and Materials Society / AIME (1996), 719,
24. D. Zander, D.L. Olson, D. Eliezer, Metal. Mat. Trans., submitted,
25. D. Zander, B. Kofmann, D. Eliezer, E.Y. Gutmanas, E. Abramov, D. Olson, in N.R. Moody, A.W. Thompson (Eds.), Hydrogen Effect on Material Behavior, TMS, Warrendale 2002, in press.
26. F.H. Froes, D. Eliezer, H.G. Nelson, The Minerals, Metals, and Materials Society / AIME, (1996), p 719.
27. W.R. Kerr: Metal Trans. 16A (1985), p 1077.
28. N. Bailey, F.R. Coe, T.G. Gooch, P.H.M. Hard, N. Jenkins and R.J. Pargeter, "Welding Steels without Hydrogen Cracking," Abington Publishing, Cambridge, 1989.
29. N. Yorioka and H. Suzuki, "Hydrogen Assisted Cracking in C-Mn and Low Alloy Steel Weldments", Intl. Matls. Review, vol. 35, no. 4, 1990, p.217.
30. E. Baune, "High Performance Basic Flux-Cored Arc Welding Consumable Development," M.S. Thesis, Colorado School of Mines, July 19, 1999.
31. I.K. Pokhodnya, "Hydrogen Behavior in Welded Joints," *Hydrogen Management in Steel Weldments*, ed. by J.L. Davidson and D.L. Olson, DSTO, WTIA, Melbourne, Australia, 1996, pp. 145-181.
32. M. Eberhart, Private Communication, Colorado School of Mines.
33. I.S. Maroef, "Fundamentals of Hydrogen Trapping in Iron", Phd. Thesis Dissertation, Colorado School of Mines, 1999.
34. Y. Fukai, "The Metal-Hydrogen System", Springer-Verlag, Berlin, Germany (1993).
35. N.Eliaz, D. Fuks, and D. Eliezer, "A New Model for the Diffusion Behavior of Hydrogen in Metallic Glasses", pp 1-9, Elsevier Science Ltd., Great Britain, (1999).
36. A. Lasseigne, MSc thesis, (2004)

3.0 ACCOMPLISHMENTS OF THIS RESEARCH CONTRACT PERIOD

- Thermoelectric power measurements have been demonstrated to be very capable, as well as a rapid and accurate method to assess the hydrogen content in austenitic type structural materials. The hydrogen content has been correlated to TEP electronic measurements using non-destructive surface contact probes. These correlations have been made on austenitic steel, iron and monel 500. The monel 500 results showed that the hydrogen pick up due to cathodic protection of submarine propeller fasteners can be rapidly assessed by such non-destructive contact measurements.

- TEP assessment of the diffusible hydrogen content in ferritic and martinsitic steels, which means that this technique can possibly replace the existing IIW hydrogen determination practice on welded coupons. Further development is needed to make this practice applicable to welded structures. The problem is associated with the rapid hydrogen transport in the ferritic, bainitic, and martinsitic steels. A practice is required that can integrate the amount of hydrogen coming out of the steel in a short period of time and then can use a diffusion derived expression to extrapolate this result to the amount of hydrogen desorbed in three days. The period is required in the IIW standard for room temperature desorption. These developments may lead to a rapid surface contact method to assess hydrogen build up in gun barrels.

- The use of hydrogen as a transient alloying addition was used as a method to assess the influence of a small variation in a specific alloy composition on a given property. Since hydrogen donates its electron to the *d*-band in a manner similar to that of other alloying additions, the effect of certain alloy additions on a property can be assessed by diffusion of hydrogen into the alloy and perform property tests. In this research hydrogen additions successfully demonstrated that it could change the thermal expansion coefficient of Invar. This practice can offer major savings in time and expense in achieving the optimum alloy content for a specific property.

- The use of a transient hydrogen approach to enhance the plasticity during alloy forming was successfully demonstrated. Hydrogen was absorbed at elevated temperature into 2 1/4 Cr-1Mo steel and Ti-Nb alloys; the new reactive–refractory alloys. After hydrogen absorption these alloy were deformed at high temperature in compression. The formed part is then given a vacuum hydrogen desorption at elevated temperature so not to leave hydrogen in the part which could cause hydrogen cracking at room temperature. The hydrogen-enhanced plasticity in 2 1/4 Cr-1Mo steel exhibited a major reduction in the flow stress when loaded at an optimum strain rate. The 2 1/4 Cr-1Mo steel showed plasticity more related to pure iron.

- The use of hydrogen as a transient alloy addition was also evaluated on Ni-Ti alloys in a collaborative project with Ben Gurion University of the Negev (Israel) and the University of Dortmond (Germany). Hydrogen enhanced plasticity was also experienced in these reactive-refractory alloys. With further development this practice of high temperature hydrogen enhanced forming may offer a means to form alloys with limited plasticity.

- The high temperature hydrogen enhanced plasticity is apparently associated with the enhanced mobility of the dislocations. In 2 1/4 Cr-1 Mo steels the dislocations appeared to easily move around classical dislocation pinning sites; i.e. the atmosphere of fine carbide precipitate pinning sites.

- TEP and magnetic susceptibility measurements were demonstrated as an effective practice to determine the hydrogen content in hydrogen storage materials, AB2 and AB5 types. This measurement practice can be applied in a manner that is used to determine the classical temperature-composition-pressure diagram associated with hydrogen content in materials. It was found to correlate well with information found on TCP diagrams. Electronic measurement approach allows for a more rapid development of hydrogen storage alloys. This new practice offers a major accomplishment to the new Presidential Hydrogen Initiative. The evaluation of low temperature hydrogen storage materials, used in small power sources, needs both thermodynamic and kinetic data to find the optimal reversible hydrogen storage electrodes. The TEP measurements offer this capability.

- The determination of interstitial nitrogen content in nitrogen strengthened austenitic stainless steel welds utilizing a non-destructive thermoelectric power surface contact probe has been demonstrated. The use of an ester-halogen digestion technique to determine the nitrogen associated with nitrides in super austenitic stainless steel weld metal was developed and demonstrated.

- High nitrogen steel welds were found to promote sensitization due to chromium depletion adjacent to the nitrides. The thermoelectric power coefficient is very sensitive to these nitrogen driven microstructural changes, but needs careful calibration to standards. TEP can be used as a rapid non-destructive technique to assess alloy composition, phase, and microstructure variations.

4. COLLABORATIONS

In performing our research we maintain collaboration with:

Gregory Vigilante	U.S. Army Benet Laboratories
Dr. Edward Metzbower	U.S. Navy Research Laboratory
Robert DeNale	U.S. Navy, Naval Surface Warfare Center
Dr. Vinod S. Agarwala	U.S. Navy, Naval Air System Command
Dr. Calvin Hyatt	Canadian Defense, DREA
Dr. Ron Goldfarb	Magnetic Laboratory, NIST, Boulder
Prof. Victor Kaydanov	Electronic Measurement Laboratory, Physics Dept., CSM
Dr. Franz Freibert	Los Alamos National Laboratory
Dr. Alex Landau	Israeli Nuclear Center, Beer Sheva, Israel
Dr. Thomas Boellinghaus	BAM (Federal Institute of Materials Research and Testing) Berlin, Germany
Prof. Dan Eliezer	Ben Gurion University of the Negev, Beer Sheva, Israel

5. LIST OF ALL PUBLICATIONS

(a) Papers published in peer-reviewed journals

1. R.D. Smith II, G. Plandis, I. Maroef, D.L. Olson, and T.R. Wildeman, "The Determination of Hydrogen Distribution in High Strength Steel Weldments: Part I: Laser Ablation Methods", Welding Journal, vol. 80, pp. 115s-121s (2001).
2. R.D. Smith II, B.K. Benson, I. Maroef, D.L. Olson, and T.R. Wildeman, "The Determination of Hydrogen Distribution in High Strength Steel Weldments: Part II: Optoelectronic Diffusible Hydrogen Sensor", Welding Journal, vol. 80, pp. 122s-126s (2001).
3. Y.D. Park, I.S. Maroef, A. Landau, and D.L. Olson, "Retained Austenite as a Hydrogen Trap in Steel Welds", Welding Journal, vol. 81 (2), pp 27s-35s (2002).
4. R. D. Smith III, D.K. Benson, J. Roland Pitts, D.L. Olson, and T. K. Wildeman, "Fiber Optic Sensor for Measurement of Diffusible Weld Hydrogen: Measurements by Fiber Optic Sensors", Material Prufung, vol. 43, (1-2), pp. 26-29 (2001).
5. I. S. Maroef, D. L. Olson, M. Eberhart and G. R. Edwards, "Hydrogen Trapping in Ferritic Steel Weld Metal", Int. Mat. Rev., vol. 47 (4), pp. 191-223 (2002).
6. D.L. Olson, A.N. Lasseigne, M. Marya, and B. Mishra, "Weld Features that Differentiate Weld and Plate Corrosion", Practical Failure Analysis (PFANF8) Vol 3(5), pp 34-47, October (2003).
7. D. Zander, I. Maroef, D. Olson, D. Eliezer, "Positive Effects of Hydrogen on the Plasticity of 2 1/4 Cr-1Mo Steel", J. Alloys and Compounds, Vol. 365-367, pp. 809-817 (2003)
8. P. Termsuksawad, S. Niyomsoan, B. Mishra, D.L. Olson, Z.Gavra and V.I. Kaydanov, "Measurement of hydrogen in alloys by magnetic and electronic techniques" Journal of Alloys and Compounds, Vol. 373 (1-2), pp. 86-95 (2004).
9. S. Niyomsoan, W. Grant, D.L. Olson and B. Mishra, "Variation of Color in Titanium and Zircorum Nitride Decorative Thin Films", Thin Solid Films, 415, pp 187-194 (2002)
10. I.S. Maroef and D.L. Olson, "Evaluation of Hydrogen Trapping for Management in Steel Welding", in 6th Int. Trends in Welding Research Conference Proceedings, pp. 557-562, 15-19 April 2002, Pine Mountain, GA, ASM International, Materials Park, OH (2003).
11. D.L. Olson, Y.D. Park, V. Kaydanov, R.D. Smith, Z. Gravra, A. Landau, D. Zander, R.B. Goldfarb, "Advances in Hydrogen Sensors for Welds", 6th Int. Trends in Welding Research Conference Proceedings, pp. 551-556, 15-19 April 2002, Pine Mountain, GA, ASM International, Materials Park, OH (2003).
12. D. Zander, B. Kofmann, D. Eliezer, E.Y. Gutmanas, E. Abramov, D.L. Olson, "Influence of Hydrogen on Phase Stability and Microhardness in Ti-Nb", in Hydrogen Effects on Material Behavior and Corrosion Deformation Interactions, pp. 345-354, TMS, Warrendale, PA (2003)
13. C.A. Lensing, I.S. Maroef, Y.D. Park, and D.L. Olson, "Irreversible Hydrogen Traps in High Strength Steel Weld Metal", in Hydrogen Effects on Material Behavior and Corrosion Deformation Interactions, pp. 73-82, TMS, Warreldale, PA (2003).
14. D. Zander, D.L. Olson, and D. Eliezer, "Mutual Effects of Hydrogenation and Deformation in Ti-Nb Alloys", Metallurgical and Materials Transaction A, Vol. 34A, pp. 2199-2206 (2003).
15. C.A. Lensing, Y.D. Park, I.S. Maroef, D.L. Olson, Yttrium Hydrogen Trapping to Manage Hydrogen in HSLA Steel Welds, Welding Journal, Vol 83(8), 254s-266s.
16. D. Eliezer, N. Eliaz, D. Zander, and D.L. Olson, "Hydrogen-Assisted Materails Proceeding", in Hydrogen Effects on Material Behavior and Corrosion Deformation Interactions, pp. 315-328, TMS, (2003)

(b) Papers published in non-peer-reviewed journals or in conference proceedings

1. Y.D. Park, C. Lensing, I. Maroef, D.L. Olson, and Z. Gavra, "Advances in Hydrogen Management for High Strength Steel", 9th CF/DRDC MEETING on NAVAL APPLICATIONS OF MATERIALS TECHNOLOGY, Dartmouth, Nova Scotia, CANADA, p. 215-231 (2001).

2. Y.D. Park, C. Lensing, I. Maroef, D.L. Olson, and Z. Gavra, "Advances in Hydrogen Management for High Strength Steel", Proceedings of 9th CF/DRDC Meeting on Naval Applications of Materials Technology, Dartmouth, Nova Scotia, Canada, pp 215-231, Defence Research Establishment Altantic, Special Report DREA SR 2001-094, June (2001).
3. D.L. Olson, B. Mishra, R. D. Smith II, S. Niyomsoan, P. Termsuksawad, Y.D. Park, V. Kaydanov, Z. Gavra, and R.B. Goldfarb "Advances in Weld Hydrogen Sensors, Intern. Conference on Joining of Advanced and Specialty Materials IV, pp. 118- 124, ASM Materials Solution Conference and Exposition, November 5-8, 2001, Indianapolis, IN, ASM, Materials Park, OH. (2002).
4. D. L. Olson, D. Zander, B. Mishra, Z. Gavra, R. D. Smith, and Y. D. Park, " Advanced Analytical Approach to Determine Hydrogen Contents in Welds", Proc. Int. Conf. on Technological and Research Developments in Welded Defence Equipment, paper 16, pp. 1-11, Melbourne, Victoria, Australia, 18-19 March 2002, WTIA, Silverton, NSW, 1811 (2002).
5. P. Termsuksawad, S. Niyomsoan, B. Mishra, R. B. Goldfarb, D. L. Olson, and Z. Gavra, Measurement of Hydrogen by Magnetic and Electronic Techniques in Metallic Materials, 201st Electrochemical Society Meeting, Philadelphia, PA., 13 pages, May 12-17, (2002).
6. B. Mishra, D.L. Olson, P. Termsuksawad, "Sensing of Hydrogen in Advanced Ni-MH Battery Materials", in Advanced Materials for Energy Conversion II, pp. 111-118, TMS, Warrendale, PA (2004).
7. Y.D. Park, D.L. Olson, Z. Gavra, and B. Mishra, "Characterization and Prediction of Hydrogen Absorption Behavior for AB5 type Hydrogen Storage Alloys by Using Electronic Measurement", in 6th Int. Conf. on New Energy Systems and Conversions, Pusan, pp. 69-75 (2003).

(c) Papers presented at meetings, but not published in conference proceedings

1. D.L. Olson, S. Liu, Y.D. Park, and J.C. Madeni, "Advances in Hydrogen Management for High Strength Steel", Proc. Of Int. Conf. on Welding and Joining of Materials, October 27-29, 2003, Lima, Peru (2003).

(d) Manuscripts submitted, but not published

6. LIST OF ALL PARTICIPATING SCIENTIFIC PERSONNEL

David L. Olson Professor & Principal Investigator

Angelique Lasseigne (Completed MSci, Aug 04, PhD student)
(TEP Nitrogen Assessment of Nitrogen Strengthened Stainless Steels and TEP Assessment of Residual Stresses)

Yeong-Do Park (Completed PhD, August 03)
(Use of TEP Measurements for Microstructural Analysis)

Termsuksawad (Completed PhD, May 03)
(AB_5 Hydrogen Storage Research)

Saisa Niyomsoan (Completed PhD, August 03)
(AB_2 Hydrogen Storage Research)

Joseph Cisler MSci student
(Sensing of Weld Hydrogen)